Prickle and Ror modulate Dishevelled-Vangl interaction to regulate non-canonical Wnt signaling during convergent extension

Hwa-seon Seo[1*#], Deli Yu[1*], Ivan Popov[1], Jiahui Tao[1], Allyson Angermeier[1], Bingdong Sha[1], Jeffrey D. Axelrod[2], Chenbei Chang[1] and Jianbo Wang[1@]

[1] Department of Cell, Developmental and Integrative Biology, University of Alabama at Birmingham, 1918 University Blvd., Birmingham, AL 35294

[2] Department of Pathology, Stanford University School of Medicine, Stanford, CA, 94305

* These authors contributed equally to this work.

[@] Correspondence: j18wang@uab.edu

[#] Current address: iCura Diagnostics, 107 Great Valley Parkway, Malvern, PA 19355

Abstract

Convergent extension (CE) is a fundamental morphogenetic process where oriented cell behaviors lead to polarized extension of diverse tissues. In vertebrates, regulation of CE requires both non-canonical Wnt, its co-receptor Ror, and “core members” of the planar cell polarity (PCP) pathway. PCP was originally identified as a mechanism to coordinate the cellular polarity in the plane of static epithelium, where core proteins Frizzled (Fz)/ Dishevelled (Dvl) and Van Gogh-like (Vangl)/ Prickle (Pk) partition to opposing cell cortex. But how core PCP proteins interact with each other to mediate non-canonical Wnt/ Ror signaling during CE is not clear. We found previously that during CE, Vangl cell-autonomously recruits Dvl to the plasma membrane but simultaneously keeps Dvl inactive. In this study, we show that non-canonical Wnt induces Dvl to transition from Vangl to Fz. PK inhibits the transition, and functionally synergize with Vangl to suppress Dvl during CE. Conversely, Ror is required for the transition, and functionally antagonizes Vangl. Biochemically, Vangl interacts directly with both Ror and Dvl. Ror and Dvl do not bind directly, but can be cofractionated with Vangl. We propose that Pk assists Vangl to function as an unconventional adaptor that brings Dvl and Ror into a complex to serves two functions: 1) simultaneously preventing both Dvl and Ror from ectopically activating non-canonical Wnt signaling; and 2) relaying Dvl to Fz for signaling activation upon non-canonical Wnt induced dimerization of Fz and Ror.

Introduction

Throughout the animal kingdom, convergent extension (CE) is a universal morphogenetic engine that reshapes tissues during embryogenesis (Davey and Moens, 2017; Goodrich and Strutt, 2011; Huebner and Wallingford, 2018; Keller, 2002). Through polarized cell intercalation, directional cell migration or oriented cell division, CE generates powerful morphogenetic force to elongate a tissue in one direction while simultaneously narrowing it in the perpendicular direction. Disruption of CE can disturb normal embryogenesis from flies to mammals and causes various congenital disorders, including neural tube defects and skeletal disorders such as Robinow Syndrome and Brachydactyly type B (Butler and Wallingford, 2017; Wang et al., 2012; Yang and Mlodzik, 2015).

In vertebrates, CE is regulated by genes in the planar cell polarity (PCP) pathway. PCP refers to cell polarity orthogonal to that of apical-basal in epithelial cells. It was initially discovered in *Drosophila* as a signaling mechanism coordinating polarized cellular structures in the plane of the epithelium. The PCP pathway consists of six core proteins in flies, including three transmembrane proteins (the atypical cadherin Flamingo (Fmi), the receptor Frizzled (Fz), and the four-pass transmembrane protein Van gogh (Vang; Vangl in vertebrates)), and three cytoplasmic proteins (Dishevelled (Dsh; Dvl in mammals), Diego (Dgo), and Prickle (Pk)). A key feature of the core PCP proteins is that they assemble into two distinct complexes, those of Fmi/Fz/Dsh/Dgo and Fmi/Vang/Pk, that localize asymmetrically on opposing cell cortexes. Extensive genetic and imaging studies in flies, combined with computational modeling, have led to a model of feedback interaction in establishing core PCP protein distribution. The model proposes that Fmi on neighboring cells can establish homophilic interaction to facilitates cross talk between extracellular Fz and Vang in trans at the cell-cell junctions, with Dsh, Dgo and Pk function to stabilize the interacting complexes across the cell junctions. At the same time, these cytoplasmic proteins destabilize the juxtaposition of Fz and Vang in the same cell to segregate the complexes. Several mechanisms are used to facilitate both positive and negative feedback regulations, including selective interaction with partner proteins, post-translational modification of different components, stability of core proteins at cell junctions, transport of components along cytoskeleton, and membrane protein recycling and subcellular localization (Cho et al., 2015; Ressurreicao et al., 2018; Shimada et al., 2006; Strutt et al., 2013; Warrington et al., 2017). These feedback mechanisms act together to promote asymmetric clustering of Fz/Dsh/Dgo and Vang/Pk complexes at the distal and proximal cell junctions, respectively, to regulate asymmetric cytoskeletal organization and to coordinate planar polarity across the entire epithelium (Amonlirdviman et al., 2005; Axelrod and Tomlin, 2011; Humphries and Mlodzik, 2018; Strutt et al., 2016).

Though the PCP components are conserved in vertebrates, they modulate cell polarity not only in the plane of epithelial cells, but also in actively migrating cells, including neurons, neural crest, metastatic cancer cells, and cells undergoing CE. These cells share dynamic behaviors with constantly changing cell-cell contacts and interactions. Asymmetric localization of individual PCP proteins has been reported in a number of such cells, but the pattern varies and segregation of PCP complexes has not been consistently observed (reviewed in (Davey and Moens, 2017)). Moreover, as the majority of these studies focus on the activities of individual PCP component in regulating polarized cell behaviors, less is known about how PCP proteins interact with each other to coordinately control the migratory processes (Davey and Moens, 2017).

Potential differences in PCP protein interaction and function in *Drosophila* and vertebrates have emerged from some recent studies. While mutual inhibition between *Vangl* and *Fz/Dvl* is expected based on the *Drosophila* work, a number of reports also reveal a functional synergy between these proteins in mice. For instance, simultaneous decrease in gene dosage of *Vangl2* and *Dvl* enhanced CE defects in neural tube closure and cochlea elongation, and compound mice mutants in *Vangl2* and several *Fz* genes show similar more exacerbated defects than those with mutations in individual genes (Etheridge et al., 2008; Wang et al., 2006; Yu et al., 2010; Yu et al., 2012). Upstream of Fz, the requirement of Wnt ligand in fly PCP signaling was debated initially (Chen et al., 2008; Wu et al., 2013), and disproved more recently (Ewen-Campen et al., 2020; Yu et al., 2020). In contrast, non-canonical Wnts, including Wnt5a and 11, are essential for CE in vertebrates (Grumolato et al., 2010; Heisenberg et al., 2000; Yamaguchi et al., 1999), and a functional synergy between Vangl2 and Wnt5a has been shown in development of multiple tissues in mice (Gao et al., 2011; Qian et al., 2007; Sinha et al., 2012; Wang et al., 2011). These findings, which collectively implicate a positive role of Vangl in Wnt/Fz/Dvl mediated non-canonical Wnt signaling activation, bring up an essential question on how Vangl may both cooperate with and inhibit Wnt/Fz/Dvl.

A further complication of non-canonical Wnt/ PCP signaling during vertebrate development is the involvement of several co-receptors including Ror1/2, Ptk7 and Ryk, whose functions are not linked to fly PCP ((Ripp et al., 2018); reviewed in (Green et al., 2014)). For instance, Ror2 has been shown to bind to Wnt5a together with Fz and is required to mediate Wnt5a-induced phosphorylation of Dvl in mammals (Grumolato et al., 2010; Ho et al., 2012; Nishita et al., 2010). Mouse mutants deficient in Ror1/2 phenocopy many defects of *Wnt5a* mutants (Ho et al., 2012), demonstrating a critical function of this co-receptor family in Wnt5a/ PCP signaling. Intriguingly, reduced gene dosages of both *Ror2* and *Vangl2* can lead to more severe morphogenesis defects than mutants of each individual genes, revealing a functional synergy between Vangl2 and Ror2. This is reminiscent of the functional synergy observed between Vangl2 and Wnt/Fz/Dvl. Ror2 was reported to interact with Vangl2 biochemically, and proposed to form a “receptor complex” with Vangl2 in response to Wnt5a (Gao et al., 2011). However, the biochemical and cell biological activities of the Ror2/ Vangl complex and how this may affect Wnt/Fz/Dvl PCP signaling is not understood in detail.

To understand feedback regulation of core PCP proteins in vertebrate CE, we have used the mouse and the *Xenopus* models to investigate functional and biochemical interactions of these proteins. Our previous work suggested that Vangl2 has dual activity in modulating Dvl function: it binds and recruits Dvl to the plasma membrane cell-autonomously and keeps it inactive, but at the same time enriching Dvl at this subcellular domain for optimal Fz signaling upon stimulation by the Wnt11 ligand which triggers release of Dvl from Vangl2 (Seo et al., 2017). In the current study, we attempted to address two questions raised by this model: 1) how will Vangl's molecular partner Pk modulate Vangl-Dvl interaction during CE; and 2) if Dvl is sequestered by Vangl, how can it gain access to Fz in the response to Wnt?

In flies, Pk clusters with Vang to the proximal cell junction and is required to generate feedback amplification for asymmetric localization of both Vang and Dsh/Fz. Pk is shown to stabilize Fz-clusters on the plasma membrane in neighboring cells, but destabilizes Fz-clusters in a Dsh-dependent manner through endocytosis in the same cell (Warrington et al., 2017). Competitive binding of Pk to Dsh to prevent its plasma membrane recruitment by Fz has been proposed as a mechanism to destabilize Fz/Dsh clustering in the same cell (Tree et al., 2002). But binding between Pk and Dsh was reported to be quite weak (Bastock et al., 2003), and over-expressing Pk in *Xenopus* cannot effectively abolish Fz7-mediated recruitment of Dvl to the plasma membrane (Takeuchi et al., 2003; Veeman et al., 2003). These studies thus do not fully support the notion of competitive binding to Dvl as the underlying mechanism for Pk to destabilize Fz clusters or its action during CE.

In this study, we used gastrulating *Xenopus* embryos as a CE model to carry out functional, biochemical and cell biological studies, and found that Pk helps Vangl2 to sequester both Dvl2 and Ror2, whereas Ror2 is needed for Dvl to transition from Vangl to Fz in response to non-canonical Wnt. We propose a novel model in which Pk assists Vangl to function as an unconventional adaptor that brings Dvl and Ror2 into a complex to serves two functions: 1) simultaneously preventing both Dvl and Ror2 from ectopic activation; and 2) relaying Dvl to Fz via Ror2 upon non-canonical Wnt activation. We propose that these two actions together help to modulate the threshold and dynamics of signaling activation in response to non-canonical Wnt.

Results

Pk synergizes with Vangl2 to suppress Dvl during CE

To probe the functional network of core PCP proteins during CE, we first studied how Pk interacts with Vangl2 and Dvl to regulate *Xenopus* body axis elongation in both gain- and loss-of-function scenarios. To overexpress Pk in *Xenopus* embryos, we used two different mRNAs that encode either a GFP tagged mouse Pk2 (mPk2) or a Flag-tagged *Xenopus* Pk1 (XPk) (Takeuchi et al., 2003; Vladar et al., 2012). Similar to the previous report (Takeuchi et al., 2003), we found that injecting *Xpk* or *mPk2* mRNA into the dorsal marginal zone (DMZ) of 4-cell stage *Xenopus* embryos can block CE in a dose dependent manner (Suppl. Fig. 1a and data not shown). Measurement of the length-to-width ratio (LWR) indicates that 1 and 2 ng *pk* mRNA injection can reproducibly cause moderate and severe CE defects, respectively, but 0.5 ng *Xpk* only results in a slight LWR reduction that is not statistically significant (Suppl. Fig. 1a').

With co-injection of mRNAs, however, even a very small dose of 0.1 ng *Xpk* is sufficient to cause sever CE defects together with 0.1 ng mouse *Vangl2* (*mVangl2*), which produces only a moderate CE defect when injected by itself (Fig. 1a, a'). Similarly, co-injecting 0.25 ng *mPk2*, which causes no CE defects by itself, also significantly enhances the CE defect induced by 0.1 ng *mVangl2* (Fig. 1b, b').

Conversely, we found that knocking down endogenous XPk level using antisense morpholino (*Xpk*MO, Suppl. Fig. 1b-d') can rescue *mVangl2* over-expression induced CE defect (Fig. 1c, c'), whereas over-expressing Pk can dose-dependently rescue *Xvangl2* morpholino (*XV*MO) knockdown-induced CE defect (Fig. 1d, d'). These gain- and loss-of-function results together demonstrate that Pk functionally synergize with Vangl during CE.

We then tested how Pk may affect Dvl function during CE. When co-injected, *mPk2* or *Xpk* can dose-dependently rescued the CE defects induced by *Dvl2* over-expression (Fig. 1e-f'), suggesting that Pk functionally antagonizes Dvl during CE. Together with our previous finding that Vangl exerts bimodal regulation of Dvl (Seo et al., 2017), these results suggest that Pk may synergize with Vangl to suppress Dvl function during CE. Consistent with this idea, we found that the severe CE defects induced by *Pk* and *Vangl2* co-injection could be rescued by overexpressing *Dvl2* (Fig. 1g, g').

Vangl interaction with and recruitment of Pk to the plasma membrane is essential for their functional synergy

To understand how Pk synergizes with Vangl to represses Dvl, we first investigated whether they could modulate each other's protein levels. It was reported that Vang could control Pk stability indirectly through ubiquitination in flies (Cho et al., 2015; Strutt et al., 2013), while in zebrafish Pk could down-regulate Dsh/Dvl protein level (Carreira-Barbosa et al., 2003). In our *Xenopus* experiments, however, morpholino knockdown of *Xvangl2* or over-expression of *mVangl2* did not affect the protein level of co-injected mPk2 or XPk (Suppl. Fig. 2a, b, c). In contrast, co-transfecting XPk with Vangl2 in cultured HEK293T cells did lead to significant reduction of XPk protein level (Suppl. Fig. 2d, also see Pk2 down-regulation by Vangl2 in 293 cells in (Nagaoka et al., 2019)) . Therefore, Vang/Vangl2-modulation of Pk stability seems to be context-dependent, and does not account for the observed synergy between Vangl2 and Pk during *Xenopus* CE. Furthermore, over-expression of Pk does not alter the protein level of co-injected Vangl2 or Dvl2 (Suppl. Fig. 2a, b), indicating that during *Xenopus* CE Pk does not synergize with Vangl2 or antagonize Dvl2 by altering their protein stability.

To explore other mechanisms that may explain how Pk synergizes with Vangl2 to antagonize Dvl during CE, we examined the effect of Vangl2 on PK's sub-cellular localization. When GFP tagged mPk2 is expressed alone in the animal cap in *Xenopus,* it displays general cytoplasmic distribution with slight enrichment at the plasma membrane (Suppl. Fig. 3a). Co-injection of mVangl2 significantly increased plasma membrane enrichment of mPk2 (Suppl. Fig. 3b). On the other hand, morpholino knockdown of endogenous *Xvangl2* eliminated mPk2 plasma membrane enrichment, which could be restored by co-expression of a small amount of mVangl2 (Suppl. Fig. 3c, d). Together, these data indicate that Vangl2 is both necessary and sufficient to recruit Pk to the plasma membrane.

To test whether plasma membrane recruitment of Pk by Vangl is important for their functional synergy, we took advantage of a Vangl2 R177H variant identified in a patient with diastematomyelia (Kibar et al., 2011). This variant changes the highly conserved Arg177 to histidine in the intracellular loop region between TM2 (transmembrane domain) and TM3 (Fig. 2a). Importantly, this variant does not perturb plasma membrane trafficking of Vangl2 (Fig. 2b, b’), its stability (Fig. 2g, Suppl. Fig. 4e) or its ability to interact with and recruit Dvl to the plasma membrane (Suppl. Fig. 4a-d). The variant, however, reduced Vangl2 interaction with Pk and recruitment of Pk to the plasma membrane (Fig. 2c-g).

Functionally, R177H variant significantly reduced the synergy between Vangl2 and Pk during CE (Fig. 2h, i). Moreover, compared to wild-type Vangl2, Vangl2 R177H results in significantly less severe CE defects when over-expressed alone in the DMZ (Suppl. Fig. 5a, a’), and is less capable of suppressing Dvl-Fz mediated signaling activation during CE when co-expressed (Suppl. Fig. 5b, b’). We interpret these data to suggest that: 1) direct binding of Vangl2 to Pk, through which Pk is recruited to the plasma membrane, is crucial for their functional synergy during CE; and 2) direct binding of Vangl to Dvl alone may not be sufficient to suppress Dvl, and simultaneous interaction with Pk may be required for Vangl to efficiently inhibit Dvl during CE.

Pk synergizes with Vangl to sequester Dvl from Fz

To investigate how Pk may help Vangl to suppress Dvl during CE, we first tested whether Pk over-expression may disrupt Dvl interaction with Fz. In both animal cap and DMZ cells, Fz7 can recruit mCherry tagged Dvl2 (Dvl2-mCh) to the plasma membrane (Suppl. Fig. 6b, e). Co-expression of GFP-mPk2, however, does not perturb Fz7-mediated plasma membrane recruitment of Dvl2 (Suppl. Fig. 6c, f), suggesting that over-expression of Pk alone cannot effectively disrupt Dvl-Fz interaction in *Xenopus*.

We then investigated the alternative possibility that Pk may help Vangl to sequester Dvl, and thereby preventing Wnt-Fz-Dvl interaction to inhibit non-canonical Wnt signaling activation during CE. Our previous studies provided evidence that Vangl recruits Dvl into an inactive complex at the plasma membrane; and Wnt11 induction can dissociate Dvl from Vangl (Seo et al., 2017). We therefore first tested whether Pk can reinforce Vangl-Dvl interaction to counter the dissociation effect by Wnt11. Pk overexpression can indeed significantly reduce Wnt11-induced dissociation of EGFP-Vangl2 and Flag-Dvl2 in the DMZ (Suppl. Fig. 7). These data argue that Pk may strengthen Vangl-Dvl interaction to inhibit Dvl from responding to non-canonical Wnt ligands.

To further test how Vangl/Pk may regulates Dvl's response to non-canonical Wnt, we performed imaging studies. In *Xenopus* and zebrafish, Wnt11 can induce formation of Fz-Dvl complexes that cluster as patches at the cell-cell contacts (Witzel et al., 2006; Yamanaka and Nishida, 2007). We therefore investigated how Vangl/ Pk may affect formation of Wnt11-induced Fz-Dvl patches. We found that *Xenopus* Wnt11 can induce Dvl2-mCh to form distinct patches along cell-cell contacts in both animal cap (Fig. 3a-c') and DMZ cells (Suppl. Fig. 8). When GFP-tagged *Xenopus* Fz7 is co-injected, it exclusively forms membrane patches that completely overlapped with Dvl2 (Fig. 3d-f'), consistent with clustering of Fz-Dvl complexes. Co-injecting moderate level of GFP-tagged mouse Vangl2 (0.1 ng) does not perturb Wnt11-induced Dvl2 patch formation. In contrast to Fz7, Vangl2 is distributed broadly on the plasma membrane, but to our surprise it also displays overlapping enrichment with Dvl2 patches (Fig.3g-I; Suppl. Fig. 8). Close examination revealed that in most cases Vangl2 is enriched at the edges of Dvl2 patches, but diminished at the center (Fig.3g'-I', compare red arrows and arrowheads to green arrows and arrowheads). In 3-D reconstructed confocal images, enriched Vangl2 often forms rings that encircle Dvl2 patches (Suppl. Fig. 8c, white arrows; and enlarged views in a'-c').

To quantitatively assess their spatial distribution, we measured and plotted the relative intensity of Dvl2 against Fz7, Vangl2 or membrane-GFP control along the length of ten representative patches (Fig. 3p-r). Our analyses revealed that membrane-GFP displayed no enrichment along Wnt11-induced Dvl2 patches (Fig. 3p). Fz7, however, showed enrichment that correlated strongly with Dvl2: their intensities follow a similar pattern of increasing sharply from the edge and peaking coincidentally at the center of the patches. In contrast, Vangl2 enrichment starts to appear slightly outside of Dvl2 patches (Fig. 3g', i', r, green arrowheads), peaks at the edges as Dvl2 intensity begins to rise, and dips at the center where Dvl2 and Fz7 intensities reach the maximum (Fig. 3g', i', r, green arrows). These imaging analyses are consistent with our co-IP data (Suppl. Fig. 7), and further suggest the possibility that Dvl may leave Vangl and transition to Fz upon Wnt11 induction.

We then tested whether addition of Pk can help Vangl2 to counter the effect of Wnt11. Indeed, co-injecting Pk with 0.1 ng Vangl2 effectively inhibited Wnt11-induced Dvl2 patch formation, making Dvl2 more evenly distributed along the plasma membrane (Fig.3m-o) and overlap with Vangl2 (Fig.3m'-o', t). Similar inhibition of Dvl patch formation can also be achieved, albeit less effectively, by over-expression of high level Vangl2 alone (Fig.3j-I', s).

To examine how Vangl2 and Pk could affect Fz7 enrichment in the Wnt11-induced Fz/Dvl patches, we co-injected fluorescent protein-tagged Dvl2 and Fz7. Moderate over-expression of Vangl2 or Pk individually does not affect enrichment of Fz7 within Wnt11-induced Dvl2 patches (compare Fig. 4 a-c' with d-i'), but Vangl2 and Pk together not only disrupt Dvl2 patches, but also disperse Fz7 into small puncta (Fig. 4j-l'). Close examination revealed that some of the Fz7 puncta are on the plasma membrane and largely co-localize with Dvl2. The rest of Fz7 puncta, however, are located in the cytoplasm near the plasma membrane and appear to be endocytosed vesicles (Fig. 4k', l', arrows). Interestingly, these cytoplasmic puncta contain only Fz7 but not Dvl2 (compare arrows in Fig. 4j' to k').

To confirm that the cytoplasmic Fz7 puncta are endocytosed vesicles, we performed FM4-64 dye uptake experiment (Cho et al., 2015; Classen et al., 2005). FM4-64 is a membrane impermeable fluorescent dye that can only be internalized through endocytosis. When we incubated the explants with FM4-64, we found that many Fz7 puncta induced by Vangl2/Pk co-injection were also positive for FM4-64 (Suppl. Fig. 9d-f'), indicating that they are indeed endocytic vesicles.

These data imply that Pk may assist Vangl to sequester Dvl, thereby reducing the accessibility of Dvl to attenuate Fz-Dvl complex formation in response to Wnt11, and resulting in Fz destabilization at the plasma membrane. To test this idea, we reduced Dvl availability at the plasma membrane using another strategy. Over-expression of DshMA, a mitochondrial tethered Dvl, can sequester endogenous Dvl to the mitochondria (and away from the plasma membrane) through DIX-domain mediated oligomerization (Park et al., 2005). We found that DshMA injection indeed mimicked the effect of Vangl2/Pk co-injection on Fz, resulting in reduced Fz7 clustering upon Wnt11 induction, formation of cytoplasmic puncta near the plasma membrane, and diminished plasma membrane localization (Suppl. Fig. 10).

To further test whether Vangl2 needs direct interaction with PK in order to down-regulate Fz7 stability at the plasma membrane and Fz7 patch formation in response to Wnt11, we analyzed Vangl2 R177H variant that specifically reduces Vangl2-Pk interaction (Fig.2 and Suppl. Fig. 5). We found that unlike wild-type Vangl2, co-injecting Vangl2 R177H with Pk failed to significantly diminish Wnt11-induced Fz7 patch formation or cause cytoplasmic Fz7 puncta (Fig. 5). These data support the notion that direct Pk-Vangl2 interaction seems to be required for efficient sequestration of Dvl from Fz, thereby reducing Fz stability on the plasma membrane.

As a final test for this idea, we examined Dvl phosphorylation known to be inducible by Fz and non-canonical Wnt signaling activation (Axelrod, 2001; Klein et al., 2006; Rothbacher et al., 2000; Shimada et al., 2001; Strutt et al., 2019; Strutt et al., 2006). *Xenopus* extract from embryos injected with *flag-Dvl2* in the DMZ often shows Dvl2 migrating as two bands. The upper, slower migrating band increases in intensity from stage 10 to 12, correlating with the onset and progression of CE (Fig. 6a). The slower migrating form of Dvl2 is increased by Fz7 co-injection, but eliminated by phosphatase treatment (Fig. 6b). Interestingly, high level Vangl2 over-expression can reduce the phosphorylated form of Dvl2, while Fz7 can counter Vangl2's effect to increase Dvl2 phosphorylation when co-injected (Fig. 6c). Importantly, our co-IP experiment demonstrated that only the faster migrating, presumably unphosphorylated form of Dvl2 could be precipitated by Vangl2 in *Xenopus* (Fig. 6d), suggesting that Vangl2-bound Dvl2 may be shielded from Fz-induced phosphorylation. High level Pk (1 ng *Xpk*) is not sufficient to significantly reduce phosphorylated form of Dvl2 when injected alone, but can synergize with moderate level of co-injected Vangl2 to suppress Dvl2 phosphorylation (Fig 6e, f). Together with our previous findings, these data suggest that Pk facilitates Vangl2 to sequester Dvl2 from Fz and, in turn, Fz-induced phosphorylation.

Ror2 facilitates transition of Dvl2 from Vangl2 to Fz complexes in response to non-canonical Wnt

The above results prompted us to ask that if Dvl is sequestered at the plasma membrane by Vangl2/Pk, how it may shuttle to form a complex with Fz in response to non-canonical Wnt? As Ror2 has been shown to act as a non-canonical Wnt co-receptor capable of interacting with both Fz and Vangl2 during CE (Gao et al., 2011; Grumolato et al., 2010; Hikasa et al., 2002; Ho et al., 2012; Wallkamm et al., 2014), we hypothesized that Ror2 may be a key component to shuttle Dvl between Vangl2 and Fz.

To test this idea, we first examined the functional relationship between Ror2 and Vangl2. Injecting moderate amount of *Xenopus ror2* mRNA (*Xror2;* 0.05-0.1 ng) can efficiently rescue the severe CE defects induced by 0.2 ng of *Vangl2* mRNA (Suppl. Fig.11a, b), supporting the idea that like Dvl2, Ror2 antagonizes Vangl2 to activate non-canonical Wnt signaling during CE.

Secondly, we tested that at the cellular level, how Wnt11 may induce Ror2 to cluster into patches and how Ror2 patches may correlate with Dvl2 and/or Vangl2 patches. When Wnt11 is co-injected with EGFP tagged Ror2 and Dvl2-mCh, it indeed induces Ror2 to form patches that show overlap with Dvl2 patches (Fig.7a-d). Close examination of these patches revealed that Ror2, like Fz, accumulates with Dvl2 to high levels in the center of the patches (red arrowhead in Fig.7a’, d). But unlike Fz, Ror2 patches are longer and extend slightly outside of Dvl2 patches (green arrowheads in Fig.7a’, d), reminiscent of Vangl2 enrichment (Fig.3g’-i’; r) and suggesting that Ror2 and Vangl2 can accumulate together at the border of Dvl2 patches to form a complex devoid of Dvl2. Similar to Vangl2, Ror2 continues to display broad membrane distribution outside of Dvl2 patches (Fig.7a, c) in the presence of Wnt11, differing from Dvl2 and Fz that are localized almost exclusively within patches (Fig.7b,c; Fig.3d-f). These results suggest that at least under the moderate over-expression condition for the imaging experiments, a portion of

Ror2 remains bound to Vangl2 on the plasma membrane whereas most Dvl2 dissociates from Vangl2 to form the signaling patches in response to Wnt11.

To test whether Ror2 is required for Dvl2 patch formation in response to Wnt11, we used a verified morpholino to knock down endogenous XRor2 (Schambony and Wedlich, 2007) and found that Dvl2 patch formation is significantly diminished in Xror2 morphants (Fig.7e, f). Collectively, these data indicate that Ror2, a molecular partner of Vangl2, is an obligatory component of the Fz/Dvl cluster induced by Wnt11.

To further scrutinize the molecular mechanism, we tested biochemically whether Ror2 is required for Dvl2 to dissociate from Vangl2 in response to Wnt11. Indeed, we found that Wnt11-induced dissociation of Dvl2 from Vangl2 was significantly reduced when endogenous Ror2 level was knocked down by *Xror2*-MO (Supplementary Fig. 12a).

Together, these data support the notion that Ror2 is required for Dvl2 to transition from Vangl2 to Fz in response to Wnt11. To test how Ror2 may facilitate this transition, we performed co-IP experiment. Similar to the previous report (Gao et al., 2011), our co-IP experiment detected Ror2 interaction with Vangl2 but not Dvl2 (Suppl. Fig. 12b), suggesting that Ror2 may bind directly to Vangl2 but not Dvl2. As Ror2 and Dvl2 can both bind to Vangl2, we reasoned that they could interact indirectly through their mutual binding with Vangl2. We thus performed fluorescence-detection size exclusion chromatography (FSEC) with protein extract from Xenopus embryos injected with *Xror2-EGFP*, *HA-Vangl2* and *Flag-Dvl2*. The elution of Ror2-EGFP was monitored by a fluorescence detector following size exclusion chromatography. The fractions of different molecular size were collected and analyzed by western blot. We found co-fractionation of Ror2, Vangl2 and Dvl2 in fractions 14, 15 and16 (with the approximate molecular weight of 773-1717, 348-773 and 166-348 kD, respectively; Supplementary Fig. 12c).

This result supports our hypothesis that Ror2, Vangl2 and Dvl2 form complexes *in vivo*. We envision a model in which an Ror2/Vangl2/Dvl2 complex serves two purposes during CE: it allows Vangl2 to simultaneously sequester both Ror2 and Dvl2 and keeps them inactive, while in response to non-canonical Wnt it enables Ror2 to shuttle Dvl to Fz (See Fig.9 and Discussion below).

Bimodal regulation of Ror2 by Vangl2/Pk during non-canonical Wnt signaling

We used Wnt11-induced patch formation as a functional test for the above model. First, we test whether Vangl2 may synergize with Pk to sequester Ror2 from Fz7 as it does to Dvl2 (Fig. 3 and 4). When fluorescent protein-tagged Ror2 and Fz7 are co-expressed with Wnt11, they form clusters that co-localize. Moderate over-expression of Vangl2 or XPk individually does not affect Ror2/Fz7 co-clustering within Wnt11-induced patches (compare Fig.8a-c' with d-i'). Vangl2 and Pk co-injection, however, significantly diminished Ror2/Fz7 patches induced by Wnt11 and caused Fz7 to form intracellular vesicles near the plasma membrane (Fig.8k', l', arrows). Interestingly, like Dvl2 (Fig.4j', k'), Ror2 is not present in these endocytosed Fz7 vesicle (compare arrows in Fig.8j' to k') but remained on the plasma membrane, presumably with Dvl2.

We then tested whether Vangl2 may also be required for Ror2 to form Wnt11-induced patches with Fz7 since our model predicts that, by bridging Ror2 and Dvl into a complex, Vangl2 helps Ror2 to shuttle Dvl to Fz in response to non-canonical Wnt (Fig. 9). We found that partial knockdown of endogenous *XVangl2* with *XV*MO indeed diminished Ror2/Fz7 patches formed in response to Wnt11 (Fig.8m-o') with simultaneous formation of Fz7 intracellular vesicles around the plasma membrane (Fig.8m', n', arrows), similar to co-overexpression of Vangl2 and XPk (Fig.8k', l'). Collectively, these data support our model and suggest that with Pk, Vangl2 exerts bimodal regulation of Ror2 in non-canonical Wnt signaling.

Discussion

Early fly studies identified six proteins that act as core members to coordinate cellular polarity across the plane of the epithelium. In-depth genetic, biochemical and imaging studies have subsequently elucidated how the six core PCP proteins interact within and between cells to establish feedback loops that partition Vang/Pk and Fz/Dsh/Dgo clusters on opposing cell cortexes (Amonlirdviman et al., 2005; Goodrich and Strutt, 2011). These studies establish a foundation to understand the action of PCP proteins in static epithelial cells. They do not, however, seem to provide direct explanation for how PCP proteins regulate polarized and dynamic cell behavior during CE, where asymmetric partitioning of core PCP proteins has not been consistently observed and non-core PCP proteins, including non-canonical Wnts and co-receptor Ror1/2, are also critically involved. We previously provided evidence that during CE, Vangl exerts bimodal regulation of Dvl by cell-autonomously recruiting Dvl to the plasma membrane in an inactive state, and simultaneously poising Dvl for activation upon binding of Fz to non-canonical Wnt ligands (Seo et al., 2017). In the current study, we further tested this model and demonstrated that Pk functionally synergizes with Vangl2 to inhibit Dvl2 during CE in *Xenopus*. Mechanistically, Pk binding to Vangl2 helps Vangl2 to sequester Dvl and constrain its transition to Fz. Moreover, Pk seems to play a similar role in assisting Vangl2 to sequester Ror2, whereas Ror2 is required for Dvl2 to transition from Vangl to Fz in response to non-canonical Wnt. We propose an updated model for the bimodal regulation in which Vangl2/Pk bring both Dvl2 and Ror2 into an inactive complex that prevents ectopic non-canonical Wnt signaling. On the other hand, this complex can also be coupled with Fz upon non-canonical Wnt mediated interaction between Ror2 and Fz, delivering Dvl to Fz to initiate non-canonical Wnt signaling (Fig. 9). Therefore, Vangl mediated plasma membrane recruitment of Dvl and pre-assembly of Dvl and Ror into a complex can also accelerate non-canonical Wnt signaling activation by facilitating Dvl presentation to activated Fz. Our model provides a new framework to decipher how core PCP proteins are integrated with non-core proteins to tightly control the threshold and dynamics of non-canonical Wnt/ PCP signaling during CE.

Regulation of Vangl-Dvl interaction by Pk to suppress non-canonical Wnt signaling

Our previous work proposed that Vangl-Dvl interaction provides a key switch to the central logic of PCP by enriching Dvl around the plasma membrane for effective access to Fz, while at the same time keeping Dvl inactive to prevent ectopic signaling (Seo et al., 2017). In the current study, we found that the Vangl2 R177H variant (Kibar et al., 2011), which can traffick properly and bind to and recruit Dvl2 to the plasma membrane like wild-type Vangl2 does (Fig. 2, Suppl. Fig. 4), no longer efficiently inhibits CE and rescues Fz/Dvl induced CE defect when over-expressed (Suppl. Fig.5). The results suggest that binding to Dvl *per se* is not sufficient for Vangl2 to suppress Dvl during CE. Interestingly, Vangl2 R177H displays significantly reduced binding and functional synergy with Pk. We therefore reason that interaction with Pk is necessary for Vangl2 to efficiently sequester Dvl from Fz or downstream targets like Daam1. Our biochemical and imaging experiments provide supporting evidence to this idea (Fig. 3-5; Suppl. Fig. 7).

There are at least three possibilities accounting for how Pk can assist Vangl2 to sequester Dvl. First, given that Dvl, Pk and Vang/Vangl can mutually interact with each other (Bastock et al., 2003; Humphries et al., 2023; Jenny et al., 2003; Takeuchi et al., 2003; Tree et al., 2002), Pk may stabilize a ternary Dvl/Pk/Vangl complex by simultaneously interacting with both Vangl and Dvl (Fig. 9a). We, however, do not favor this possibility because 1) the binding between Pk and Dvl was reported to be quite weak (Bastock et al., 2003); 2) our unpublished data show that ∆PL, a Pk mutant lacking the PET/LIM domains necessary for Dvl binding (Takeuchi et al., 2003), can largely mimic wild-type Pk function. Furthermore, a new study in flies showed that the phosphorylation status of a conserved tyrosine in the cytoplasmic tail of Vang provides opposite binding preference for Pk and Dsh, suggesting that simultaneous binding of both Pk and Dsh to the C-terminus of Vang may not be possible (Humphries et al., 2023).

Secondly, Pk may regulate biochemical modification on Vangl2 to strengthen Vangl2-Dvl interaction. The best known modification on Vang/Vangl is phosphorylation at several N-terminal serine/threonine residues in response to Wnt/Fz (Gao et al., 2011; Kelly et al., 2016; Yang et al., 2017), and a recent study in flies revealed that Pk can prevent Vang phosphorylation at these residues to decrease Vang turnover (Strutt et al., 2019). In our co-IP studies in *Xenopus*, however, we found that Wnt11 can disrupt Vangl2-Dvl2 interaction yet has no significant impact on Vangl2 band shift that was reported to be indicative of its N-terminal phosphorylation (Gao et al., 2011; Kelly et al., 2016; Strutt et al., 2019); Suppl. Fig.7a, lower panel). Conversely, although Pk over-expression can counter Wnt11-induced dissociation of Vangl2 and Dvl2, it does not seem to significantly affect Vangl2 band shift either (Suppl. Fig.7a, lower panel). These results are consistent with a previous report that, in fly S2 cells, Pk over-expression does not alter Vang N-terminal phosphorylation (Kelly et al., 2016). While our current study provides no evidence to support that Pk modulates Vangl N-terminal phosphorylation to regulate Vangl-Dvl interaction, this possibility remains an interesting idea and should be tested in the future using the reported phosphomutant and phosphomimetic Vangl2 (Yang et al., 2017). Finally, phosphorylation of a conserved C-terminal tyrosine residue of Vang was recently reported to decrease its binding with Dsh (Humphries et al., 2023), and could therefore provide a mechanism to control Vangl-Dvl interaction. But the regulatory mechanism of this tyrosine phosphorylation is not clear and does not seem to depend on Fz. Further studies will be needed to elucidate the role of this tyrosine phosphorylation in vertebrate CE.

Thirdly, Pk binding may induce allosteric change or clustering of Vangl to increase the overall avidity for Dvl binding. Vang/Vangl is able to dimerize, and possibly oligomerize into larger cluster through their C-terminal tail and/or transmembrane domains (Belotti et al., 2012; Jenny et al., 2003). Interestingly, quantitative imaging studies in flies have revealed that in stable PCP clusters, the ratio between Vang and Pk is 6:1 (Strutt et al., 2016). In light of our data suggesting that the intracellular loop between TM2 and 3 in Vangl2 may form another Pk binding site in addition to the canonical Pk binding domain at the C-terminal tail (Fig. 2; (Bastock et al., 2003; Jenny et al., 2003), it is tempting to speculate that Pk may nucleate or stabilize Vangl oligomer formation through multimeric interactions with different domains on multiple Vangl proteins. Such oligomeric Vangl cluster may form a “cage” to more effectively sequester Dvl due to increased local concentration and/or higher binding affinity resulted from conformational change upon oligomerization or Pk binding.

Our above model seemingly contradicts with the fly studies showing that Vang/Pk clusters are partitioned to the opposite cell cortexes from Fz/Dsh clusters and are clearly devoid of Dsh. These segregated clusters, however, seem to form progressively from initial symmetrically distributed PCP proteins along cell-cell junctions at early stages where Vang does co-localize with Dsh (Bastock et al., 2003), and a new study further implicated the functional importance of Vang-Dsh binding in fly PCP establishment (Humphries et al., 2023). Persistent contact and stable junctions between neighboring cells may facilitate feedback interaction to partition Vang/Pk from Dsh/Fz (Stahley et al., 2021). In dynamically moving cells during CE, intercellular feedback interactions are likely limited and transient, therefore posing challenges for stable segregation of distinct PCP clusters. Conversely, non-canonical Wnts play a key role during vertebrate CE but not in fly PCP establishment. These differences may lead to some changes in the molecular actions of PCP proteins (see below).

An Ror-dependent relay mechanism to deliver Dvl for non-canonical Wnt signaling

The premise of our model is that during CE, Vangl acts via a relay mechanism to bring Dvl to the plasma membrane, and then releases Dvl to Fz during PCP activation. Pk may tighten up this relay mechanism, via regulating Vangl-Dvl interaction, to increase the efficiency of Dvl plasma membrane recruitment and the threshold at which Dvl can be released to Fz. While the detailed mechanisms for how Dvl can be released from Vangl and transitioned to Fz are yet to be elucidated in further details in the future, our studies identified several factors that contribute to the transition: non-canonical Wnt, the co-receptor Ror2 and Dvl phosphorylation.

Our co-IP and imaging studies showed that Wnt11 can trigger dissociation of Dvl2 from Vangl2 (Fig. 3g-I'; Suppl. Fig.7; (Seo et al., 2017)) and formation of Fz7-Dvl2 clusters at cell-cell contact (Fig. 3d-f'), indicating that non-canonical Wnt can act extracellularly to initiate the transition of Dvl from Vangl to Fz. It is possible that Wnt binding to Fz can directly induce events in favor of Fz-Dvl association. We, however, also consider the alternate possibility that Wnt binding to the co-receptors Ror1/2 to bring Dvl to Fz.

Like Fz, Ror1/2 also harbor the extracellular cysteine-rich domains known to interact with Wnts and have been shown to heterodimerize with Fz in response to non-canonical Wnt binding (Grumolato et al., 2010). At the same time, like Dvl, Ror2 was reported to bind directly with Vangl2 (Gao et al., 2011). We therefore postulate that Ror2 may shuttle between Vangl and Fz to deliver Dvl in a Wnt dependent manner. We note several intriguing links between Ror2 and Dvl2: 1) they both bind to Vangl2 yet display functional antagonism against Vangl2 during CE in over-expression assays (Fig. 1; Suppl. Fig. 11); 2) they both cluster with Fz in response to Wnt11 (Fig. 3, 7, 8), and importantly Ror2 is required for Dvl2 to dissociate from Vangl2 and cluster with Fz in response to Wnt11 (Fig. 7b; Suppl. Fig. 12). While Ror2 does not seem to bind Dvl directly, they both interact with Vangl2 and our SEC data show that Ror2, Vangl2 and Dvl2 co-fractionate (Suppl. Fig. 12), suggesting that they may form complexes together. Therefore, we envision a model where Vangl acting as an adaptor to bring together Dvl and Ror, either through simultaneous binding of both Dvl and Ror to a single Vangl (Fig. 9a) or self-oligomerization of Vangl proteins bound separately to Dvl and Ror (Fig. 9b). When non-canonical Wnt induces Fz-Ror to heterodimerize, the complexes consisting of Ror/Vangl/Dvl can be brought close to Fz to deliver Dvl and initiate non-canonical Wnt signaling (Fig. 9a',b').

In this model, Vangl acts as an unconventional adaptor to simultaneously serve two critical functions: it pre-assembles Ror and Dvl into complexes at the plasma membrane ready to initiate non-canonical Wnt signaling, but at the same time keeps both inactive to prevent ectopic signaling activation. We previously demonstrated that Vangl2 can prevent Dvl from interacting with its downstream effector Daam1 (Seo et al., 2017), and our data in this study suggest that Vangl/Pk may act together to sequesters both Dvl and Ror from Fz as well (Fig. 4 and 8). Based on this model, Vangl2 over-expression will exert excessive suppression to prevent non-canonical Wnt signaling during CE, which can be overcome by co-overexpressing Dvl2 or Ror2 (Fig. 1; Fig.8; Suppl. Fig. 11). Conversely, reducing the dosage of endogenous Vangl2 may decrease the assembly of Ror/Vangl/Dvl complexes, compromising signaling activation in response to non-canonical Wnt (Fig.8). Therefore, our model can explain how partial loss of Vangl2 can synergize with loss of positive non-canonical Wnt signaling regulators, including Ror2, Dvl2 and Wnt5a, to cause various severe CE defects reported in the literature (Gao et al., 2011; Qian et al., 2007; Wang et al., 2011; Wang et al., 2006).

Lastly, our data implicated an intriguing role for Dvl phosphorylation in the transition from Vangl to Fz. We found that flag-Dvl2 phosphorylation is increased as CE progresses in *Xenopus* and can be elevated by Fz7 but suppressed by Vangl2 (Fig. 6b, c). In agreement with our over-expression data in *Xenopus*, loss of both Vangl1 and 2 leads to increased Dvl2 and 3 phosphorylation in cell culture (Mentink et al., 2018). Intriguingly, Vangl2 seems to bind only to unphosphorylated form Dvl2 (Fig. 6d). These observations suggest that either Dvl phosphorylation *per se* or another associated modification can be used as a mechanism to decouple Dvl from Vangl. In support of this view, the basic region and PDZ domain of Dsh/Dvl, which mediates Dvl-Vangl interaction (Park and Moon, 2002), is a strong target of CK1 during PCP signaling in flies (Klein et al., 2006; Strutt et al., 2019; Strutt et al., 2006).

Taken together, we propose the second piece of our model (Fig. 9c, c') that during CE, non-canonical Wnt triggers association of Ror1/2 and Fz to simultaneously accomplish two events: 1) bringing Vangl-sequestered Dvl close to Fz; and 2) activating CK1 to phosphorylate Dvl. The combined effects lead to Dvl dissociation from Vangl and transition to Fz in a spatially and temporally controlled manner. On the other hand, by assisting Vangl to sequester Dvl, Pk can suppress the noise from basal CK1 activity, and allow cells to respond more specifically and dynamically to non-canonical Wnt singling during CE.

Figure legend:

Figure 1. PK synergize with Vangl to suppress Dvl during CE

Injecting 0.1 ng mouse *Vangl2* mRNA (*mVangl2*) into the DMZ results in moderate CE defects and reduction of the length-to-width ration (LWR), and the phenotypes are significantly enhanced by co-injecting a small dose of *Xpk* (a, a') or *mPk2* (b, b') mRNA that causes minimal or no CE defect *per se*. On the other hand, higher dose *mVangl2* (0.15 ng) induced more severe CE defects can be rescued by knocking down endogenous Pk using *Xpk*MO (c, c'); whereas knockdown of endogenous *vangl2* (*XV*MO) induced CE defects can be rescued by moderate mPk2 overexpression (d, d'). Conversely, 0.5 ng mouse *Dvl2* injection induced CE defects can be dose-dependently rescued by *mPk2* (e, e') and *Xpk* (f, f') co-overexpression; and mVangl2-mPk2 co-overexpression induced severe CE defect can be rescued by co-injecting Dvl2 (g, g').

Figure 2. Vangl2 RH variant diminishes membrane recruitment of Pk and reduces functional synergy with Pk

Schematic illustration showing the structure of the tetraspan protein Vangl2 and location of the R177H variant at the intracellular loop region between transmembrane domain 2 and 3 (a). When expressed in *Xenopus* animal cap cells, EGFP-Vangl2 RH displays plasma membrane localization, indistinguishable from wild-type EGFP-Vangl2 (b, b'). Immunostaining shows that flag-XPk displays diffuse cytoplasmic localization with some membrane enrichment when expressed alone (c, c'). The plasma membrane localization of flag-XPk is enhanced significantly by co-expression of wild-type Vangl2 (d, d'), but only modestly by Vangl2 RH variant (e, e'). (f) Quantification of the ratio of plasma membrane vs. cytoplasmic flag-XPk in (c), (d) and (e). Co-IP and western blot show that binding to flag-XPk is reduced by Vangl2 RH variant (g). Functionally, co-injection of 0.05 ng *Vangl2* and 0.5 ng *Xpk* can strongly synergize to disrupt CE, but the synergy is significantly reduced when *Vangl2 RH* variant mRNA is co-injected with *Xpk* (h). The CE phenotype is quantified by the LWR measurement in (i).

Figure 3. Pk synergizes with Vangl2 to inhibit Wnt11-induced formation of Dvl patches

0.25 ng *Wnt11* injection with 0.5 ng of mCh-tagged mouse *Dvl2* and membrane-GFP induces formation of distinct Dvl2 patches at the cell-cell contact (a-c'). Co-injection indicates that these Dvl2 patches completely overlap with Fz7 (d-f'). In contrast, Vangl2, when expressed at moderate levels, is distributed more broadly along the plasma membrane (g-i), but also displays enrichment immediately outside and at the edge of Dvl2 patches (g'-I', arrowheads and arrows, respectively). High level of *Vangl2* injection inhibits Wnt11-induced Dvl2 patch formation and makes Dvl2 more evenly distributed with Vangl2 (j-l'). The same effect can also be achieved by co-expressing Pk with moderate level of Vangl2 (m-o'). (p-t) Measurement of the relative intensity of Dvl2 along the patches with either membrane GFP, Fz7, Vangl2 at moderate (0.1 ng) and high (0.5 ng) levels, or Vangl2 (0.1 ng) and XPk (0.5 ng) co-injection.

Figure 4. Pk helps Vangl2 to inhibit Wnt11-induced clustering of Fz7-Dvl2 complexes

Wnt11 induces formation of overlapping Fz7 and Dvl2 patches at the cell-cell contact (a-c'). These patches are not affected by over-expressing moderate level of Vangl2 (d-f') or Pk (g-i') individually. Vangl2 and Pk co-expression, however, not only disrupt Dvl2 patches but also disperse Fz7 patches into small puncta (j-l). Enlarged views revealed that some of the Fz7 puncta are on the plasma membrane and remain co-localized with Dvl2, while the others are located in the cytoplasm near the plasma membrane (k'', l', arrows) and contain only Fz7 but not Dvl2 (compare arrows in j' to k').

Figure 5. Vangl2 R177H variant fails to synergize with Pk to inhibit Fz patch formation and down-regulate Fz stability at the plasma membrane

Wnt11 induced formation of Fz7-GFP patches on the plasma membrane (a, a') was not affected by moderate expression either wild-type Vangl2 (b, b') or Vangl2 R177H variant (c, c') alone. Pk co-injection synergized with wild-type Vangl2 to diminish Fz7 patch formation and induce cytoplasmic Fz7 puncta (d, d'), but the synergy was not observed with Vangl2 R177H (e, e').

Figure 6. Pk synergize with Vangl2 to prevent Fz-induced phosphorylation of Dvl. In *Xenopus* extract, DMZ injected Dvl2 migrates as two bands, with the slower migrating band increasing in intensity from stage 10 to 12 as CE starts and progresses during gastrulation (a). The slower migrating form of Dvl2 is increased by Fz7 co-injection, but eliminated by phosphatase treatment (b). High level Vangl2 injection can reduce the phosphorylated form of Dvl2, while Fz7 can counter Vangl2's effect to increase Dvl2 phosphorylation (c). Co-IP experiment indicates that only the faster migrating, unphosphorylated form of Dvl2 can be co-immunoprecipitated by Vangl2 (d). High level *Xpk* (1 ng) or moderate *Vangl2* (0.25 ng) cannot significantly reduce phosphorylated form of Dvl2 when injected individually, but their co-injection can suppress Dvl2 phosphorylation (e). (f) Quantification of the ratio between the fast migrating/ unphosphorylated and the slow migrating/ phosphorylated forms of Dvl2 in (e).

Figure 7. Ror2 is an obligatory component of the Fz/Dvl cluster complex induced by Wnt11. (a-c) Co-injection of *Wnt11* with EGFP-tagged *Xror2* (0.1 ng) and *Dvl2-mCh* shows that Ror2 and Dvl2 both form patches that largely overlap, but unlike Dvl2, Ror2 additionally displays broad distribution along the entire cell cortex. (c'-e') The enlarged views show that both Ror2 and Dvl2 accumulate at the center of the patches (red arrowhead), but Ror2 patches are slightly longer and extend beyond the border of Dvl2 patches (green arrowheads). (d) Measurement of the relative intensity of Dvl2-mCh along the patches with Ror2-EGFP. (e) Injection of *Wnt11* induces co-injected Dvl2-mCh to cluster into patches on the cell cortex. (b) Co-injection of 25 ng *X*ror2 morpholino (*Xror2*-MO) blocks Wnt11-induced Dvl2 clustering.

Figure 8. Vangl2/Pk exert bimodal regulation of Ror2 in non-canonical Wnt signaling. (a-c) Wnt11 induces injected XRor2-td-Tomanto and Fz7-GFP to co-cluster into patches on the cell cortex. Overexpression of Vangl2 (d-f) or Pk (g-i) individually does not perturb co-clustering of Ror2 with Fz7 in response to Wnt11, but their co-overexpression (j-l) diminishes Ror2-Fz7 co-clustering into patches and cause Fz7 to form cytoplasmic puncta whereas Ror2 remained on the plasma membrane (compare arrows in j'-l'). a'-l' are enlarged view of a-l, respectively. Conversely, partial knockdown of endogenous *XVangl2* with moderate level of *XV*MO (14 ng) also diminished Ror2/Fz7 patches formed in response to Wnt11 (Fig.8m-o') with simultaneous formation of intracellular vesicles around the plasma membrane which contain Fz7 but not Ror2 (Fig.8m'-o', arrows).

Figure 9. An integrated model for how core PCP proteins mediates non-canonical Wnt signaling to regulate CE. (a, a') In the absence of non-canonical Wnt, Pk helps Vangl to act as an adaptor that brings together Dvl and Ror, through either simultaneous binding of both Dvl and Ror to a single Vangl (a) or oligomerization of Vangl proteins bound separately to Dvl and Ror (a'), and keeps both Dvl and Ror inactive to prevent ectopic non-canonical Wnt signaling. (b, b') Non-canonical Wnt initiates signaling by triggering Fz-Ror heterodimerization, and in turn, the complexes consisting of Ror/Vangl/Dvl are brought close to Fz to deliver Dvl for activation of downstream targets. (c, c') Non-canonical Wnt also induces other events such as Dvl phosphorylation, likely through CK1, that may cause Dvl dissociation from Vangl and transition to Fz in a spatially and temporally controlled manner.

Materials and Method

Xenopus embryo manipulation and animal cap/DMZ explants

Embryos were acquired by superovulation, maintained in 0.1% MMR solution until the stages for microinjection. Morpholinos or *in vitro* synthesized RNAs were injected into either the animal side of two-cell-stage embryos or the DMZ of four-cell-stage embryos. For phenotypic analysis, the DMZ-injected embryos were fixed at tailbud stages, and the dorsal view of embryos was captured using a Leica DFC 490 camera. Phenotypic severity was quantified by calculating the length and width ratio. The length was determined by drawing a line along the long axis to measure the maximal distance from the head to the tail of each embryo. The width was measured as the average of two lines drawn perpendicular to the long axis, at the one third and two thirds length of each embryo. For animal cap elongation assay, ectodermal explants were isolated at stages 9-10 and incubated in 0.5 MMR solution containing 10 ng/ml of Activin B (R&D cat# 659-AB-005). The CE phenotype was quantified by measuring the length of the resulting explants. For fluorescent imaging to determine protein localization, DMZ or animal cap explants from injected embryos were isolated at stage 10-10.5, coversliped and subjected to confocal imaging analysis as described (Seo et al., 2017).

Co-immunoprecipitation and westernblot

RNAs or morpholinos injected embryo or explants were lysed as described for biochemistry experiments (Seo et al., 2017; Tien et al., 2015). For co-immunoprecipitation assay, protein lysates were subjected to pull-down with anti-flag antibody (Sigma Anti-FLAG M2 Magnetic Beads (Cat# 8823)). Western blot detection of proteins was carried out with anti-GFP antibody (Santa Cruz Biotechnology GFP (B-2) (Cat# sc-9996)), anti-myc antibody (Santa Cruz Biotechnology myc Antibody(G-4) (Cat# sc-373712)), or flag antibody (Sigma Anti-flag M2 antibody (Cat# F1804)).

Fluorescence-detection size-exclusion chromatography (FSEC)

2-cell stage *Xenopus* embryos were co-injected with 3 ng Ror2-EGFP, 0.5 ng Flag-Dvl2 and 1 ng HA-Vangl2 mRNA to the animal side. Animal caps were dissected around stage 10 and cultured in 0.5 X MMR at 15 ℃ overnight. Next day 35 – 40 animal caps were lysed on ice with the 200 mL lysis buffer (50 mM Tris pH 7.5, 150 mM NaCl, 0.3% Dodecylmaltoside and Protease inhibitor (Pierce™ Protease Inhibitor)). After centrifuged at 4 ℃ 14000g for 15 min, the supernatant was collected and filtered with 0.22 mm syringe filter. 100 mL lysate was loaded onto Superose 6 Increase 10/300 GL column (Cytiva, Marlborough, MA) pre-equilibrated in SEC buffer (Tris 50 mM, pH 7.5, NaCl 150 mM, Dodecylmaltoside 0.03%). The eluted Ror2-GFP was monitored by RF-10AX fluorescence detector (Shimadzu, Japan) following size-exclusion chromatography. Fractions were collected and concentrated (Pierce™ concentrator PES 10K MWCO), and used for Western blot.

Immunofluorescence staining and quantification

RNA injected animal caps were dissected and fixed in 4% PFA for immunofluorescence staining with an anti-flag antibody. The relative protein level between the plasma membrane and cytoplasm was quantified by comparing the fluorescent intensity. Briefly, the fluorescent area was defined, and the average intensity within the area was measured by Image J to calculate the total fluorescent intensity in the defined area (plasma membrane or cytoplasm).

Protein enrichment pattern within clusters was analyzed using Olympus FLOVIEW FV1000 software. Briefly, the intensity of fluorescence was measured in each defined fluorescent cluster. Since the clusters contain different number of pixels, each pixel was numbered from one end to the other end to define the location. The largest number was normalized to 100, and each number indicating the location of the pixel was converted to percentile. Likewise, to normalize the fluorescent intensity of each pixel, the highest intensity was normalized to 100, and each pixel intensity was converted to percentile. The regression curve is used to identify the distribution pattern of every pixel intensity. 10 clusters from 5-10 embryos were used for statistical analysis.

To analyze Fz7 endocytosis, vitelline membrane of injected embryos was removed at stage 10.5, and embryos were incubated in 0.1X MMR containing 5ug/ml FM4-64FX (Thermo Fisher, Cat# F34653) for 30min at room temperature before dissection. Dissected DMZ explants were coversliped, and images were captured without fixation.

RNAs and morpholinos

XWnt11, EGFP-Vangl2, HA-Vangl2, GFP-XFz7, flag-XFz7, tdT-tomatoRor2, myc-Vangl2, Dvl2-mCherry, Dvl2-flag, GFP-mPk2, flag-XPk, flag-PL, flag-∆PL, were transcribed in vitro using mMESSAGE mMACHINE SP6 Transcription Kit (Ambion cat#1340). Xenopus Vangl2-morpholino (XVMO) and Xenopus Pk-morpholino (XPkMO) are the same as previously described (ref). The dosage of each RNA or morpholino is described in each figure.

ACKNOWLEDGEMENTS

We thank Dr. Naoto Ueno for providing the flag-XPk construct. The anti-XRor2 monoclonal antibody was obtained from the Developmental Studies Hybridoma Bank, created by the NICHD of the NIH and maintained at The University of Iowa, Department of Biology, Iowa City, IA 52242.

COMPETING INTERESTS

The authors declare no competing or financial interests.

FUNDING

This work was supported by grants R35GM131914 (J.D.A.), GM127371 (C.C.), and HL138470 and AR081646 (J.W.) from the National Institutes of Health.

Supplementary Figures:

Supplementary Figure 1.

In the DMZ, both over-expression (a, a') and morpholino knockdown (b, b') of *Xpk* can dose-dependently block CE, resulting in shorten body axes and reduced LWR. In the animal cap, *Xpk*MO knockdown can also block activin induced CE (c, c'), but the defect can be rescued by co-injecting RNA encoding mouse Pk2 (d, d').

Supplementary Figure 2.

EGFP-Vangl2, *flag-Dvl*2 and *GFP-mPk2* mRNA were injected into the DMZ, either alone or together, at 4 cell stage, and embryos were harvested at stages 10.5-11 for westernblot. Co-overexpressing Vangl2 with mPk2, or Dvl2 with mPk2, does not significantly alter each other's protein level (a). Similarly, co-overexpressing Flag-XPk with EGFP-Vangl2 in activin treated animal cap explant also does not alter each other's protein level (b). Knocking down endogenous *Xvangl2* does not alter the protein level of injected Flag-XPk either (c). Interestingly, however, co-transfecting Vangl2 with XPk into 293T cells significantly reduced XPk protein level (d).

Supplementary Figure 3.

EGFP tagged mPk2 display uniform cytoplasmic distribution with some enrichment at the plasma membrane when expressed alone in animal cap cells (a, c, and enlarged view in c). Plasma membrane enrichment of mPk2 is enhanced by co-injection of mVangl2 (b), but eliminated by morpholino knockdown of endogenous XVangl2 (d). Injecting a small amount of *mVangl2* (50 pg) could restore mPk2 plasma membrane enrichment in *XVangl2* morphants (e).

Supplementary Figure 4.

Dvl2-EGFP display uniform cytoplasmic distribution when expressed alone in *Xenopus* animal cap cells (a, a’), but co-expression with either wild-type Vangl2 (b, b’) or Vangl2 R177H variant (c, c’) recruits Dvl2-EGFP to the plasma membrane. (d) Quantification of the ratio of plasma membrane vs. cytoplasmic Dvl2-EGFP in (a), (b) and (c). Co-IP and westernblot show that binding to Dvl2 is not affected by Vangl2 RH variant (e).

Supplementary Figure 5.

When injected into the DMZ, 0.2 ng and 0.1 ng wild-type mouse *Vangl2* mRNA causes severe and moderate CE defect, respectively. *Vangl2 R177H* mRNA, however, causes significantly milder CE defect (a). (a’) Quantification of the LWR of embryos in (a). *Fz7* and *Dvl2* co-injection caused severe CE defects can be rescued by 0.1 wild-type *Vangl2*, but not by *Vangl2 R177H* (b). (b’) Quantification of the LWR of embryos in (b).

Supplementary Figure 6.

In both animal cap and DMZ cells, Fz7 can recruit Dvl2 from the cytoplasm to the plasma membrane (compare b to a, and e to d). Over-expression of Pk2 does not inhibit Fz7-mediated plasma membrane recruitment of Dvl2 (c, f).

Supplementary Figure 7.

(a) In DMZ explant, binding between flag-Dvl2 and EGFP-Vangl2 is reduced by Wnt11. But over-expression of Pk2 can prevent Wnt11-induced dissociation of Dvl2 and Vangl2. (b) Quantification of EGFP-Vangl2 co-IP efficiency from 3 separate experiments.

Supplementary Figure 8.

Moderate level of *EGFP-Vangl2* (0.1 ng) was co-injected with *Wnt11* and mCherry tagged *Dvl2*. 3D reconstruction of confocal images shows that under this condition, all Dvl2 proteins on the plasma membrane formed discrete patches at the apical cell-cell junctions (a), while Vangl2 was distributed more diffusely on the plasma membrane (b) with enrichment overlapping with Dvl2 patches (c, white arrows). Enlarged views (a'-c') show that enriched Vangl2 forms rings that encircle Dvl2 patches.

Supplementary Figure 9.

Xenopus explants were incubated with FM4-64FX, a fluorescent dye that is membrane impermeable and can only be internalized through endocytosis. In explants in which *Fz7-GFP* was co-injected only with *Wnt11*, Fz7 primarily formed patches on the cell cortex. Most of the internalized FM4-64FX puncta were devoid of Fz7, and the few Fz7 puncta were devoid of FM4-64FX (arrowheads in a-c, and enlarged views a'-c'). In contrast, in explants in which *Fz7-GFP* and *Wnt11* were co-injected with *Vangl2/Pk*, majority of the Fz7-GFP puncta are positive for FM4-64FX (arrows in d-f and enlarged views d'-f'), indicating that they were largely formed through endocytosis.

Supplementary Figure 10.

Wnt11 induces formation of Fz7 patches along the plasma membrane (a). Over-expression of DshMA, a mitochondria tethered form of Dvl that can sequester endogenous Dvl/Dsh away from the plasma membrane, inhibits Fz7 patch formation, reduces membrane level of Fz7, and results in Fz7 cytoplasmic puncta (b).

Supplementary Figure 11.

DMZ injection of 0.2 ng of *Vangl2* mRNA induces severe CE defects, which can be rescued by co-injecting 0.05 or 0.1 ng of *Xror2* mRNA (a). The severity of the CE phenotype is quantified by measuring the length-to-width ratio (b).

Supplementary Figure 12.

In *Xenopus* embryo extract, co-IP experiment shows that binding between flag-Dvl2 and HA-Vangl2 is reduced by Wnt11 (compare lane2 and 3). Knocking down endogenous XRor2 with morpholino (xRor2 MO) can prevent Wnt11-induced dissociation of Dvl2 and Vangl2 (compare lane 4 and 5) (a). (b) Co-IP experiment shows that Ror2-Flag can pull down co-injected EGFP-Vangl2 but not Myc-Dvl2. (c) Fluorescence-detection size exclusion chromatography (FSEC) with protein extract from *Xenopus* embryos injected with Ror2-EGFP, HA-Vangl2 and Flag-Dvl2. A peak of EGFP signal is detected around fraction 15 (lower panel). Western blot analyses show co-fractionation of Ror2-EGFP, HA-Vangl2 and Flag-Dvl2 in fractions 14 (approximate molecular weight 773-1717 kD), 15 (~348-773 kD) and 16 (~166-348 kD).

Reference:

Amonlirdviman, K., Khare, N.A., Tree, D.R., Chen, W.S., Axelrod, J.D., Tomlin, C.J., 2005. Mathematical modeling of planar cell polarity to understand domineering nonautonomy. Science 307, 423-426.

Axelrod, J.D., 2001. Unipolar membrane association of Dishevelled mediates Frizzled planar cell polarity signaling. Genes Dev 15, 1182-1187.

Axelrod, J.D., Tomlin, C.J., 2011. Modeling the control of planar cell polarity. Wiley Interdiscip Rev Syst Biol Med 3, 588-605.

Bastock, R., Strutt, H., Strutt, D., 2003. Strabismus is asymmetrically localised and binds to Prickle and Dishevelled during Drosophila planar polarity patterning. Development 130, 3007-3014.

Belotti, E., Puvirajesinghe, T.M., Audebert, S., Baudelet, E., Camoin, L., Pierres, M., Lasvaux, L., Ferracci, G., Montcouquiol, M., Borg, J.P., 2012. Molecular characterisation of endogenous Vangl2/Vangl1 heteromeric protein complexes. PloS one 7, e46213.

Butler, M.T., Wallingford, J.B., 2017. Planar cell polarity in development and disease. Nat Rev Mol Cell Biol 18, 375-388.

Carreira-Barbosa, F., Concha, M.L., Takeuchi, M., Ueno, N., Wilson, S.W., Tada, M., 2003. Prickle 1 regulates cell movements during gastrulation and neuronal migration in zebrafish. Development 130, 4037-4046.

Chen, W.S., Antic, D., Matis, M., Logan, C.Y., Povelones, M., Anderson, G.A., Nusse, R., Axelrod, J.D., 2008. Asymmetric homotypic interactions of the atypical cadherin flamingo mediate intercellular polarity signaling. Cell 133, 1093-1105.

Cho, B., Pierre-Louis, G., Sagner, A., Eaton, S., Axelrod, J.D., 2015. Clustering and negative feedback by endocytosis in planar cell polarity signaling is modulated by ubiquitinylation of prickle. PLoS Genet 11, e1005259.

Classen, A.K., Anderson, K.I., Marois, E., Eaton, S., 2005. Hexagonal packing of Drosophila wing epithelial cells by the planar cell polarity pathway. Developmental cell 9, 805-817.

Davey, C.F., Moens, C.B., 2017. Planar cell polarity in moving cells: think globally, act locally. Development 144, 187-200.

Etheridge, S.L., Ray, S., Li, S., Hamblet, N.S., Lijam, N., Tsang, M., Greer, J., Kardos, N., Wang, J., Sussman, D.J., Chen, P., Wynshaw-Boris, A., 2008. Murine dishevelled 3 functions in redundant pathways with dishevelled 1 and 2 in normal cardiac outflow tract, cochlea, and neural tube development. PLoS Genet 4, e1000259.

Ewen-Campen, B., Comyn, T., Vogt, E., Perrimon, N., 2020. No Evidence that Wnt Ligands Are Required for Planar Cell Polarity in Drosophila. Cell Rep 32, 108121.

Gao, B., Song, H., Bishop, K., Elliot, G., Garrett, L., English, M.A., Andre, P., Robinson, J., Sood, R., Minami, Y., Economides, A.N., Yang, Y., 2011. Wnt signaling gradients establish planar cell polarity by inducing Vangl2 phosphorylation through Ror2. Developmental cell 20, 163-176.

Goodrich, L.V., Strutt, D., 2011. Principles of planar polarity in animal development. Development 138, 1877-1892.

Green, J., Nusse, R., van Amerongen, R., 2014. The role of Ryk and Ror receptor tyrosine kinases in Wnt signal transduction. Cold Spring Harb Perspect Biol 6.

Grumolato, L., Liu, G., Mong, P., Mudbhary, R., Biswas, R., Arroyave, R., Vijayakumar, S., Economides, A.N., Aaronson, S.A., 2010. Canonical and noncanonical Wnts use a common mechanism to activate completely unrelated coreceptors. Genes Dev 24, 2517-2530.

Heisenberg, C.P., Tada, M., Rauch, G.J., Saude, L., Concha, M.L., Geisler, R., Stemple, D.L., Smith, J.C., Wilson, S.W., 2000. Silberblick/Wnt11 mediates convergent extension movements during zebrafish gastrulation. Nature 405, 76-81.

Hikasa, H., Shibata, M., Hiratani, I., Taira, M., 2002. The Xenopus receptor tyrosine kinase Xror2 modulates morphogenetic movements of the axial mesoderm and neuroectoderm via Wnt signaling. Development 129, 5227-5239.

Ho, H.Y., Susman, M.W., Bikoff, J.B., Ryu, Y.K., Jonas, A.M., Hu, L., Kuruvilla, R., Greenberg, M.E., 2012. Wnt5a-Ror-Dishevelled signaling constitutes a core developmental pathway that controls tissue morphogenesis. Proc Natl Acad Sci U S A 109, 4044-4051.

Huebner, R.J., Wallingford, J.B., 2018. Coming to Consensus: A Unifying Model Emerges for Convergent Extension. Developmental cell 46, 389-396.

Humphries, A.C., Mlodzik, M., 2018. From instruction to output: Wnt/PCP signaling in development and cancer. Curr Opin Cell Biol 51, 110-116.

Humphries, A.C., Molina-Pelayo, C., Sil, P., Hazelett, C.C., Devenport, D., Mlodzik, M., 2023. A Van Gogh/Vangl tyrosine phosphorylation switch regulates its interaction with core Planar Cell Polarity factors Prickle and Dishevelled. PLoS Genet 19, e1010849.

Jenny, A., Darken, R.S., Wilson, P.A., Mlodzik, M., 2003. Prickle and Strabismus form a functional complex to generate a correct axis during planar cell polarity signaling. EMBO J 22, 4409-4420.

Keller, R., 2002. Shaping the vertebrate body plan by polarized embryonic cell movements. Science 298, 1950-1954.

Kelly, L.K., Wu, J., Yanfeng, W.A., Mlodzik, M., 2016. Frizzled-Induced Van Gogh Phosphorylation by CK1epsilon Promotes Asymmetric Localization of Core PCP Factors in Drosophila. Cell Rep 16, 344-356.

Kibar, Z., Salem, S., Bosoi, C.M., Pauwels, E., De Marco, P., Merello, E., Bassuk, A.G., Capra, V., Gros, P., 2011. Contribution of VANGL2 mutations to isolated neural tube defects. Clin Genet 80, 76-82.

Klein, T.J., Jenny, A., Djiane, A., Mlodzik, M., 2006. CKIepsilon/discs overgrown promotes both Wnt-Fz/beta-catenin and Fz/PCP signaling in Drosophila. Current biology : CB 16, 1337-1343.

Mentink, R.A., Rella, L., Radaszkiewicz, T.W., Gybel, T., Betist, M.C., Bryja, V., Korswagen, H.C., 2018. The planar cell polarity protein VANG-1/Vangl negatively regulates Wnt/beta-catenin signaling through a Dvl dependent mechanism. PLoS Genet 14, e1007840.

Nagaoka, T., Furuse, M., Ohtsuka, T., Tsuchida, K., Kishi, M., 2019. Vangl2 interaction plays a role in the proteasomal degradation of Prickle2. Sci Rep 9, 2912.

Nishita, M., Itsukushima, S., Nomachi, A., Endo, M., Wang, Z., Inaba, D., Qiao, S., Takada, S., Kikuchi, A., Minami, Y., 2010. Ror2/Frizzled complex mediates Wnt5a-induced AP-1 activation by regulating Dishevelled polymerization. Mol Cell Biol 30, 3610-3619.

Park, M., Moon, R.T., 2002. The planar cell-polarity gene stbm regulates cell behaviour and cell fate in vertebrate embryos. Nature cell biology 4, 20-25.

Park, T.J., Gray, R.S., Sato, A., Habas, R., Wallingford, J.B., 2005. Subcellular localization and signaling properties of dishevelled in developing vertebrate embryos. Current biology : CB 15, 1039-1044.

Qian, D., Jones, C., Rzadzinska, A., Mark, S., Zhang, X., Steel, K.P., Dai, X., Chen, P., 2007. Wnt5a functions in planar cell polarity regulation in mice. Developmental biology 306, 121-133.

Ressurreicao, M., Warrington, S., Strutt, D., 2018. Rapid Disruption of Dishevelled Activity Uncovers an Intercellular Role in Maintenance of Prickle in Core Planar Polarity Protein Complexes. Cell Rep 25, 1415-1424 e1416.

Ripp, C., Loth, J., Petrova, I., Linnemannstons, K., Ulepic, M., Fradkin, L., Noordermeer, J., Wodarz, A., 2018. Drosophila Ror is a nervous system-specific co-receptor for Wnt ligands. Biol Open 7.

Rothbacher, U., Laurent, M.N., Deardorff, M.A., Klein, P.S., Cho, K.W., Fraser, S.E., 2000. Dishevelled phosphorylation, subcellular localization and multimerization regulate its role in early embryogenesis. EMBO J 19, 1010-1022.

Schambony, A., Wedlich, D., 2007. Wnt-5A/Ror2 regulate expression of XPAPC through an alternative noncanonical signaling pathway. Developmental cell 12, 779-792.

Seo, H.S., Habas, R., Chang, C., Wang, J., 2017. Bimodal regulation of Dishevelled function by Vangl2 during morphogenesis. Human molecular genetics 26, 2053-2061.

Shimada, Y., Usui, T., Yanagawa, S., Takeichi, M., Uemura, T., 2001. Asymmetric colocalization of Flamingo, a seven-pass transmembrane cadherin, and Dishevelled in planar cell polarization. Current biology : CB 11, 859-863.

Shimada, Y., Yonemura, S., Ohkura, H., Strutt, D., Uemura, T., 2006. Polarized transport of Frizzled along the planar microtubule arrays in Drosophila wing epithelium. Developmental cell 10, 209-222.

Sinha, T., Wang, B., Evans, S., Wynshaw-Boris, A., Wang, J., 2012. Disheveled mediated planar cell polarity signaling is required in the second heart field lineage for outflow tract morphogenesis. Developmental biology 370, 135-144.

Stahley, S.N., Basta, L.P., Sharan, R., Devenport, D., 2021. Celsr1 adhesive interactions mediate the asymmetric organization of planar polarity complexes. Elife 10.

Strutt, H., Gamage, J., Strutt, D., 2016. Robust Asymmetric Localization of Planar Polarity Proteins Is Associated with Organization into Signalosome-like Domains of Variable Stoichiometry. Cell Rep 17, 2660-2671.

Strutt, H., Gamage, J., Strutt, D., 2019. Reciprocal action of Casein Kinase Iepsilon on core planar polarity proteins regulates clustering and asymmetric localisation. Elife 8.

Strutt, H., Price, M.A., Strutt, D., 2006. Planar polarity is positively regulated by casein kinase Iepsilon in Drosophila. Current biology : CB 16, 1329-1336.

Strutt, H., Thomas-MacArthur, V., Strutt, D., 2013. Strabismus promotes recruitment and degradation of farnesylated prickle in Drosophila melanogaster planar polarity specification. PLoS Genet 9, e1003654.

Takeuchi, M., Nakabayashi, J., Sakaguchi, T., Yamamoto, T.S., Takahashi, H., Takeda, H., Ueno, N., 2003. The prickle-related gene in vertebrates is essential for gastrulation cell movements. Current biology : CB 13, 674-679.

Tien, C.L., Jones, A., Wang, H., Gerigk, M., Nozell, S., Chang, C., 2015. Snail2/Slug cooperates with Polycomb repressive complex 2 (PRC2) to regulate neural crest development. Development 142, 722-731.

Tree, D.R., Shulman, J.M., Rousset, R., Scott, M.P., Gubb, D., Axelrod, J.D., 2002. Prickle mediates feedback amplification to generate asymmetric planar cell polarity signaling. Cell 109, 371-381.

Veeman, M.T., Slusarski, D.C., Kaykas, A., Louie, S.H., Moon, R.T., 2003. Zebrafish prickle, a modulator of noncanonical Wnt/Fz signaling, regulates gastrulation movements. Current biology : CB 13, 680-685.

Vladar, E.K., Bayly, R.D., Sangoram, A.M., Scott, M.P., Axelrod, J.D., 2012. Microtubules enable the planar cell polarity of airway cilia. Current biology : CB 22, 2203-2212.

Wallkamm, V., Dorlich, R., Rahm, K., Klessing, T., Nienhaus, G.U., Wedlich, D., Gradl, D., 2014. Live imaging of Xwnt5A-ROR2 complexes. PloS one 9, e109428.

Wang, B., Sinha, T., Jiao, K., Serra, R., Wang, J., 2011. Disruption of PCP signaling causes limb morphogenesis and skeletal defects and may underlie Robinow syndrome and brachydactyly type B. Human molecular genetics 20, 271-285.

Wang, J., Hamblet, N.S., Mark, S., Dickinson, M.E., Brinkman, B.C., Segil, N., Fraser, S.E., Chen, P., Wallingford, J.B., Wynshaw-Boris, A., 2006. Dishevelled genes mediate a conserved mammalian PCP pathway to regulate convergent extension during neurulation. Development 133, 1767-1778.

Wang, J., Sinha, T., Wynshaw-Boris, A., 2012. Wnt signaling in mammalian development: lessons from mouse genetics. Cold Spring Harb Perspect Biol 4.

Warrington, S.J., Strutt, H., Fisher, K.H., Strutt, D., 2017. A Dual Function for Prickle in Regulating Frizzled Stability during Feedback-Dependent Amplification of Planar Polarity. Current biology : CB 27, 2784-2797 e2783.

Witzel, S., Zimyanin, V., Carreira-Barbosa, F., Tada, M., Heisenberg, C.P., 2006. Wnt11 controls cell contact persistence by local accumulation of Frizzled 7 at the plasma membrane. J Cell Biol 175, 791-802.

Wu, J., Roman, A.C., Carvajal-Gonzalez, J.M., Mlodzik, M., 2013. Wg and Wnt4 provide long-range directional input to planar cell polarity orientation in Drosophila. Nature cell biology 15, 1045-1055.

Yamaguchi, T.P., Bradley, A., McMahon, A.P., Jones, S., 1999. A Wnt5a pathway underlies outgrowth of multiple structures in the vertebrate embryo. Development 126, 1211-1223.

Yamanaka, H., Nishida, E., 2007. Wnt11 stimulation induces polarized accumulation of Dishevelled at apical adherens junctions through Frizzled7. Genes Cells 12, 961-967.

Yang, W., Garrett, L., Feng, D., Elliott, G., Liu, X., Wang, N., Wong, Y.M., Choi, N.T., Yang, Y., Gao, B., 2017. Wnt-induced Vangl2 phosphorylation is dose-dependently required for planar cell polarity in mammalian development. Cell Res 27, 1466-1484.

Yang, Y., Mlodzik, M., 2015. Wnt-Frizzled/planar cell polarity signaling: cellular orientation by facing the wind (Wnt). Annu Rev Cell Dev Biol 31, 623-646.

Yu, H., Smallwood, P.M., Wang, Y., Vidaltamayo, R., Reed, R., Nathans, J., 2010. Frizzled 1 and frizzled 2 genes function in palate, ventricular septum and neural tube closure: general implications for tissue fusion processes. Development 137, 3707-3717.

Yu, H., Ye, X., Guo, N., Nathans, J., 2012. Frizzled 2 and frizzled 7 function redundantly in convergent extension and closure of the ventricular septum and palate: evidence for a network of interacting genes. Development 139, 4383-4394.

Yu, J.J.S., Maugarny-Cales, A., Pelletier, S., Alexandre, C., Bellaiche, Y., Vincent, J.P., McGough, I.J., 2020. Frizzled-Dependent Planar Cell Polarity without Secreted Wnt Ligands. Developmental cell 54, 583-592 e585.

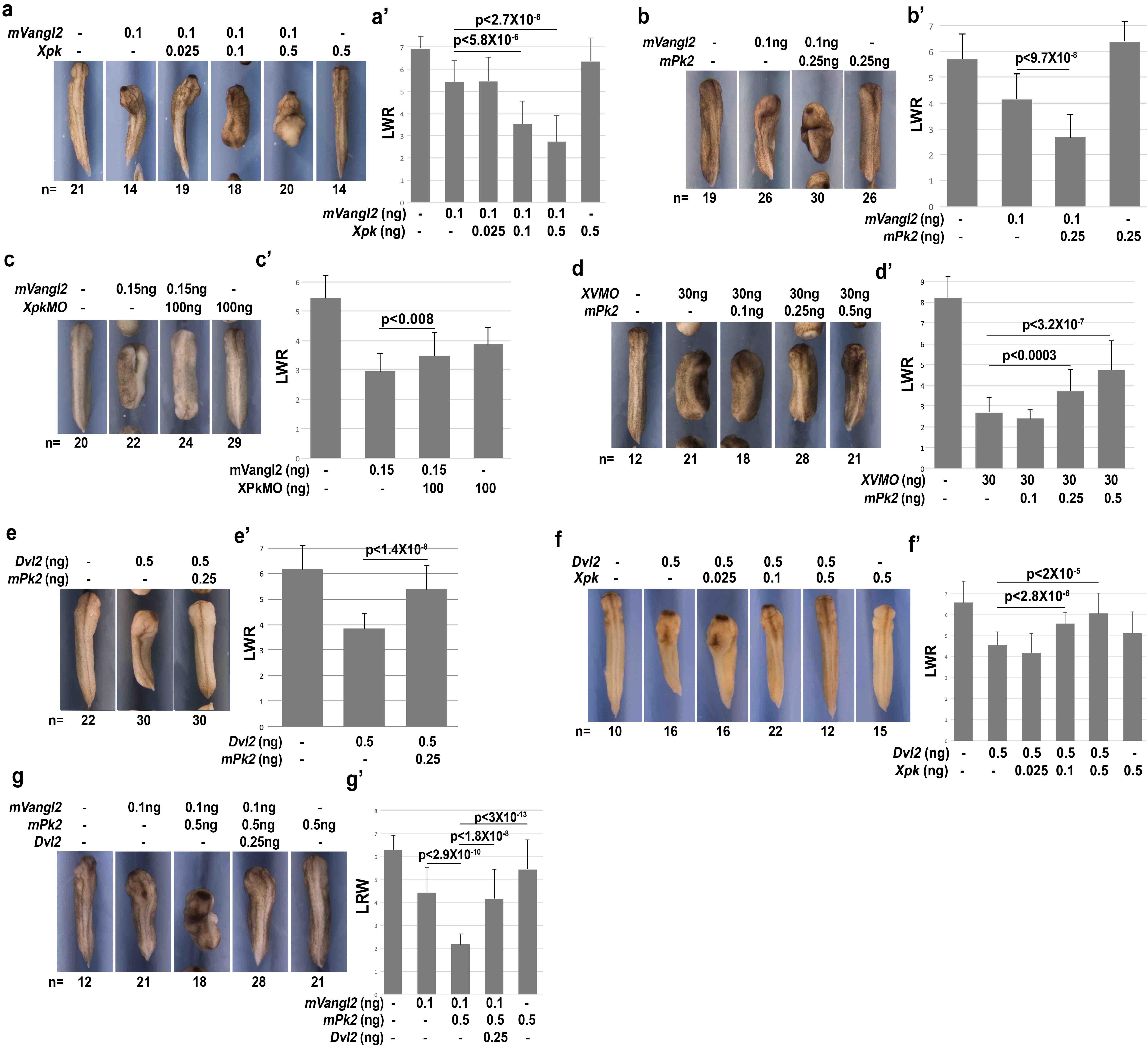

Figure 1. Pk synergize with Vangl to suppress Dvl

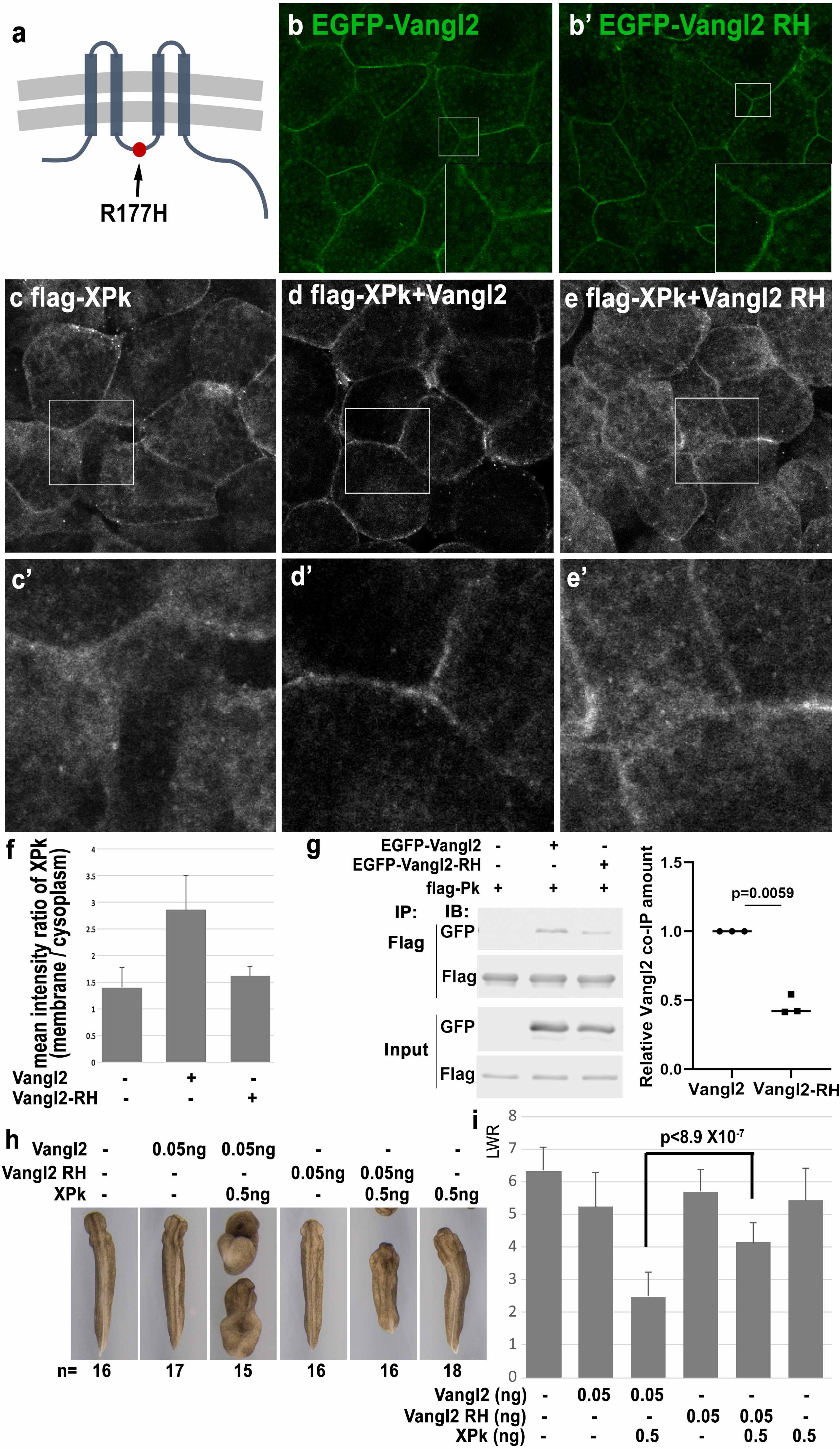
a
R177H
b EGFP-Vangl2
b' EGFP-Vangl2 RH
c flag-XPk
d flag-XPk+Vangl2
e flag-XPk+Vangl2 RH
c'
d'
e'
f
mean intensity ratio of XPk (membrane / cysoplasm)
4
3.5
3
2.5
2
1.5
1
0.5
0
Vangl2 - + -
Vangl2-RH - - +
g
EGFP-Vangl2 - + -
EGFP-Vangl2-RH - - +
flag-Pk + + +
IP:
IB:
Flag
GFP
Flag
Input
GFP
Flag
Relative Vangl2 co-IP amount
1.5
1.0
0.5
0.0
p=0.0059
Vangl2
Vangl2-RH
h
Vangl2 - 0.05ng 0.05ng - - -
Vangl2 RH - - - 0.05ng 0.05ng -
XPk - - 0.5ng - 0.5ng 0.5ng
n= 16 17 15 16 16 18
i
LWR
8
7
6
5
4
3
2
1
0
p<8.9 X10-7
Vangl2 (ng) - 0.05 0.05 - - -
Vangl2 RH (ng) - - - 0.05 0.05 -
XPk (ng) - - 0.5 - 0.5 0.5

Figure 2. Vangl2 R177H variant diminishes membrane recruitment of Pk and reduces functional synergy with Pk

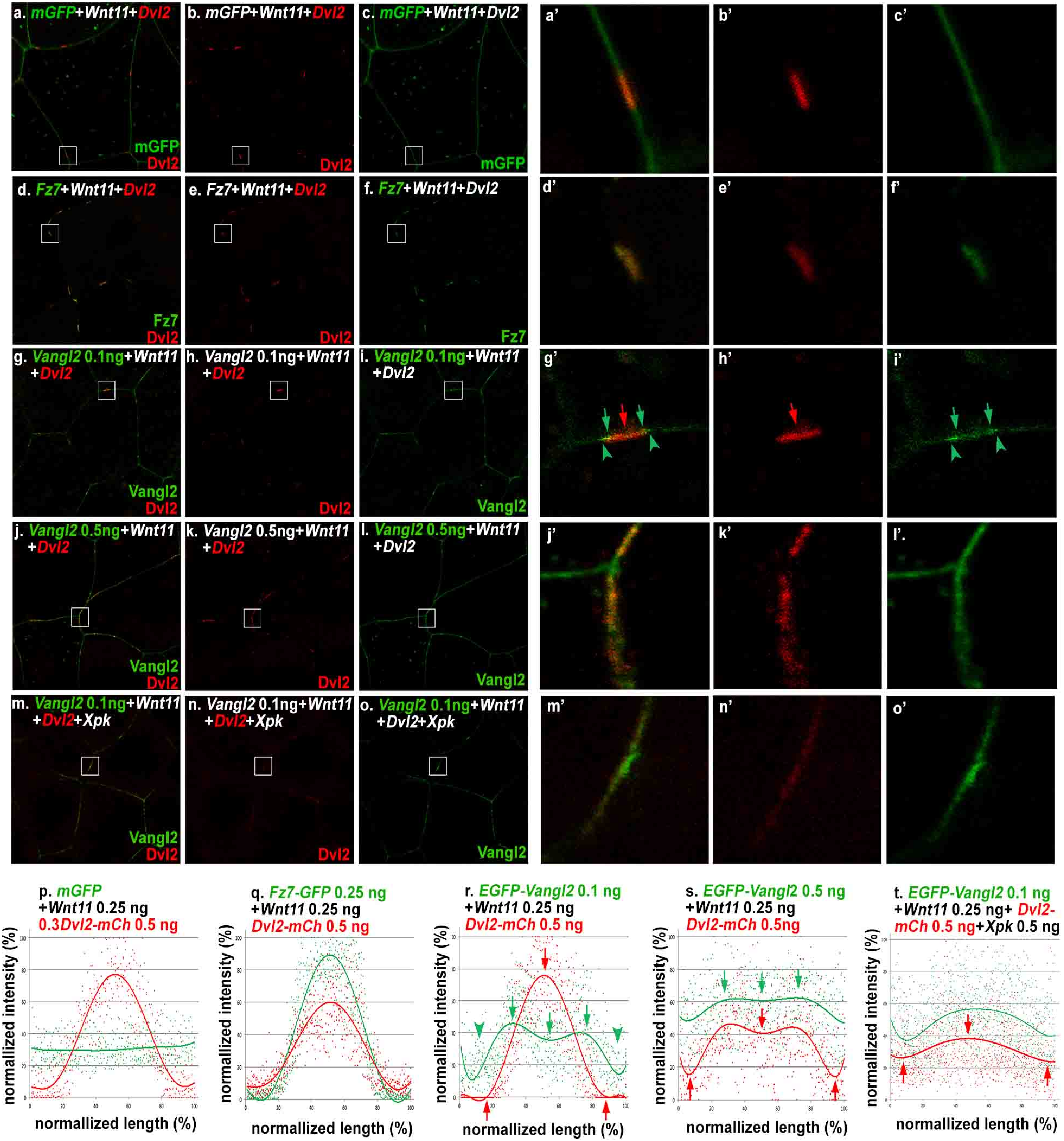
a. mGFP+Wnt11+Dvl2
mGFP
Dvl2
b. mGFP+Wnt11+Dvl2
Dvl2
c. mGFP+Wnt11+Dvl2
mGFP
a'
b'
c'
d. Fz7+Wnt11+Dvl2
Fz7
Dvl2
e. Fz7+Wnt11+Dvl2
Dvl2
f. Fz7+Wnt11+Dvl2
Fz7
d'
e'
f'
g. Vangl2 0.1ng+Wnt11 +Dvl2
Vangl2
Dvl2
h. Vangl2 0.1ng+Wnt11 +Dvl2
Dvl2
i. Vangl2 0.1ng+Wnt11 +Dvl2
Vangl2
g'
h'
i'
j. Vangl2 0.5ng+Wnt11 +Dvl2
Vangl2
Dvl2
k. Vangl2 0.5ng+Wnt11 +Dvl2
Dvl2
l. Vangl2 0.5ng+Wnt11 +Dvl2
Vangl2
j'
k'
l'.
m. Vangl2 0.1ng+Wnt11 +Dvl2+Xpk
Vangl2
Dvl2
n. Vangl2 0.1ng+Wnt11 +Dvl2+Xpk
Dvl2
o. Vangl2 0.1ng+Wnt11 +Dvl2+Xpk
Vangl2
m'
n'
o'
p. mGFP +Wnt11 0.25 ng 0.3Dvl2-mCh 0.5 ng
q. Fz7-GFP 0.25 ng +Wnt11 0.25 ng Dvl2-mCh 0.5 ng
r. EGFP-Vangl2 0.1 ng +Wnt11 0.25 ng Dvl2-mCh 0.5 ng
s. EGFP-Vangl2 0.5 ng +Wnt11 0.25 ng Dvl2-mCh 0.5ng
t. EGFP-Vangl2 0.1 ng +Wnt11 0.25 ng+ Dvl2-mCh 0.5 ng+Xpk 0.5 ng
normallized intensity (%)
normallized length (%)
0
20
40
60
80
100

Figure 3. Pk synergizes with Vangl2 to inhibit Wnt11-induced formation of Dvl patches

Dvl2-mCh
Fz7-GFP
merge
Dvl2-mCh
Fz7-GFP
merge
a
b
c
a'
b'
c'
Wnt11
Dvl2-mCh
Fz7-GFP
d
e
f
d'
e'
f'
Wnt11
Dvl2-mCh
Fz7-GFP
Vangl2
g
h
i
g'
h'
i'
Wnt11
Dvl2-mCh
Fz7-GFP
Xpk
j
k
l
j'
k'
l'
Wnt11
Dvl2-mCh
Fz7-GFP
Vangl2
Xpk

Figure 4. Pk helps Vangl2 to inhibit Wnt11-induced clustering of Fz7-Dvl2 complexes

Wnt11 0.3 ng
Fz7-GFP 0.1 ng
-
-
Wnt11 0.3 ng
Fz7-GFP 0.1 ng
Vangl2 0.1 ng
-
Wnt11 0.3 ng
Fz7-GFP 0.1 ng
Vangl2 RH 0.1 ng
-
Wnt11 0.3 ng
Fz7-GFP 0.1 ng
Vangl2 0.1 ng
Xpk 0.5 ng
Wnt11 0.3 ng
Fz7-GFP 0.1 ng
Vangl2 RH 0.1 ng
Xpk 0.5 ng
a
b
c
d
e
a'
b'
c'
d'
e'

Figure 5. Vangl2 R177H variant fails to synergize with Pk to inhibit Fz patch formation and down-regulate Fz stability at the plasma membrane

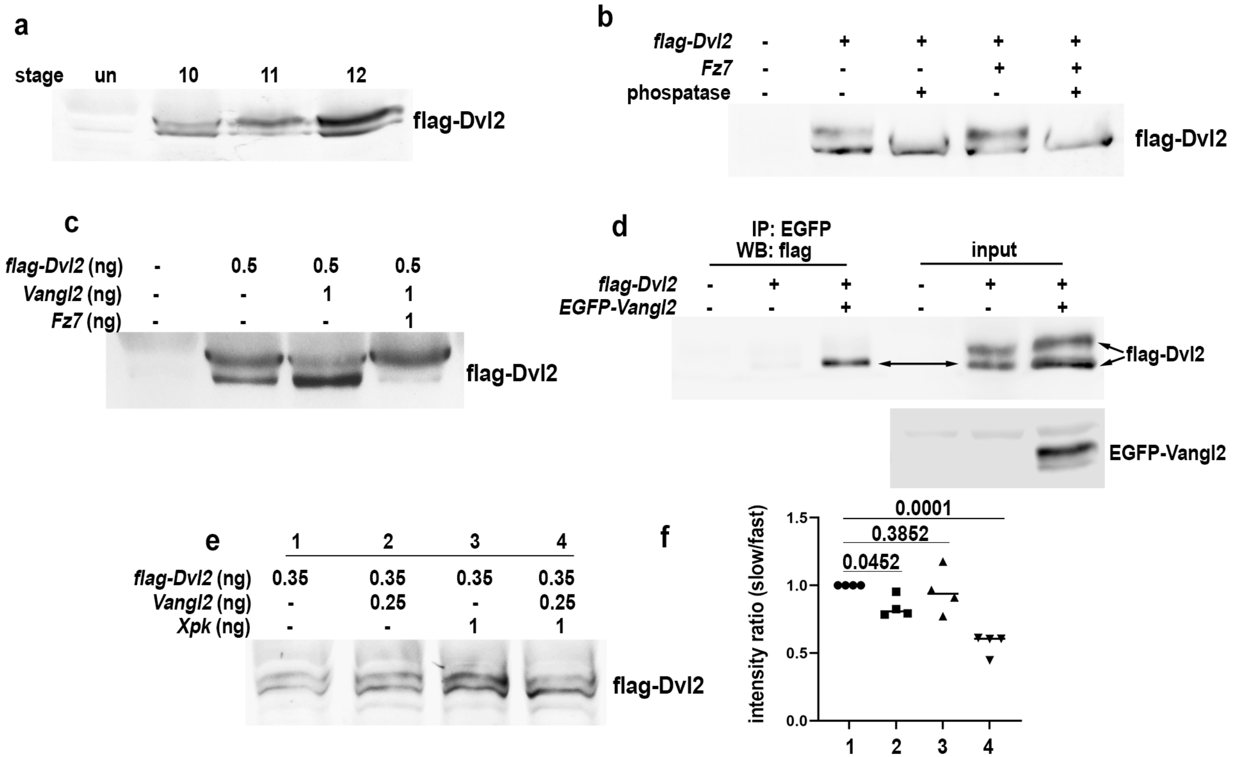

Figure 6. Pk synergize with Vangl2 to prevent Fz-induced phosphorylation of Dvl.

a. Wnt11+Xror2+Dvl2
XRor2
b. Wnt11+Xror2+Dvl2
Dvl2
c. Wnt11+Xror2+Dvl2
Xror2
Dvl2
a'
b'
e'
d
Wnt11 (0.25 ng)+Xror2-EGFP (0.1 ng)
+Dvl2-mCh (0.5 ng)
normalized intensity (%)
100
80
60
40
20
0
0
20
40
60
80
100
normalized length (%)
e. Wnt11+Dvl2
Dvl2
f. Wnt11+Xror2-MO+Dvl2
Lorem ipsum
Dvl2

Figure 7. Ror2 is an obligatory component of the Fz/Dvl cluster complex induced by Wnt11

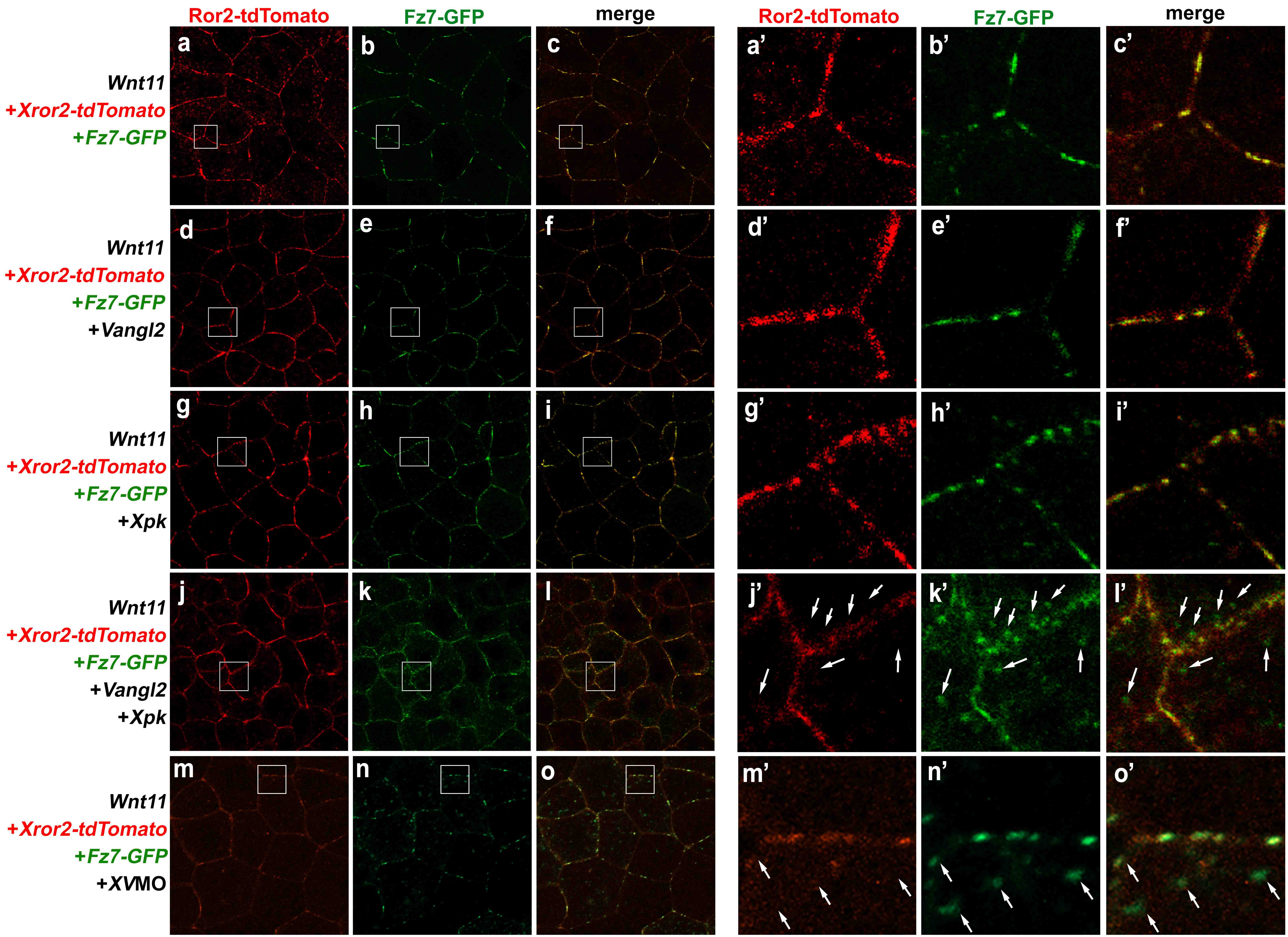
Ror2-tdTomato
Fz7-GFP
merge
Ror2-tdTomato
Fz7-GFP
merge
a
b
c
a'
b'
c'
Wnt11
+Xror2-tdTomato
+Fz7-GFP
d
e
f
d'
e'
f'
Wnt11
+Xror2-tdTomato
+Fz7-GFP
+Vangl2
g
h
i
g'
h'
i'
Wnt11
+Xror2-tdTomato
+Fz7-GFP
+Xpk
j
k
l
j'
k'
l'
Wnt11
+Xror2-tdTomato
+Fz7-GFP
+Vangl2
+Xpk
m
n
o
m'
n'
o'
Wnt11
+Xror2-tdTomato
+Fz7-GFP
+XVMO

Figure 8. Vangl2/Pk exert bimodal regulation of Ror2 in non-canonical Wnt signaling

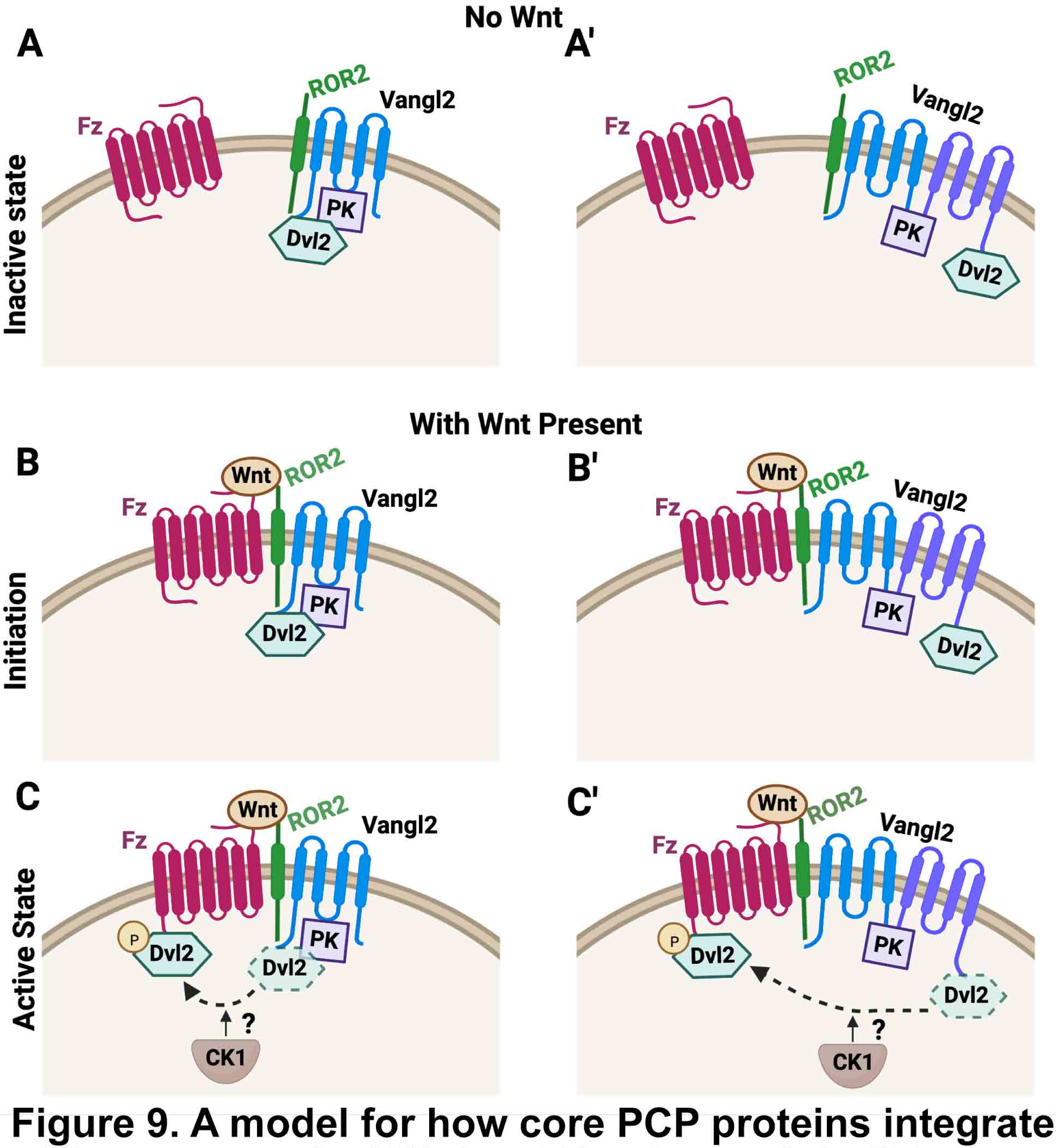
No Wnt
A
A'
Inactive state
Fz
ROR2
Vangl2
PK
Dvl2
With Wnt Present
B
B'
Initiation
Wnt
C
C'
Active State
P
CK1
?

Figure 9. A model for how core PCP proteins integrate with non-canonical Wnt and Ror to regulate CE

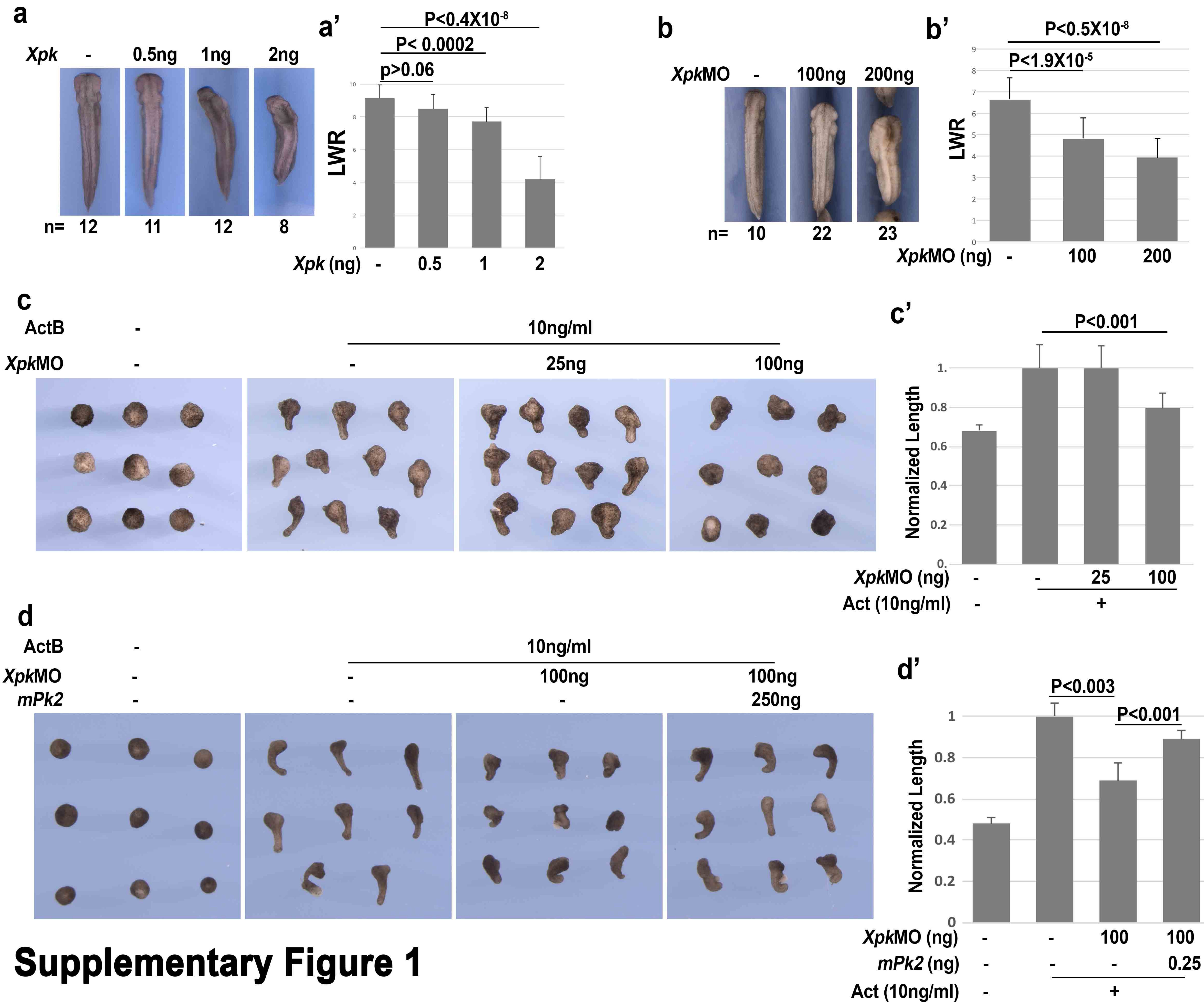

Supplementary Figure 1

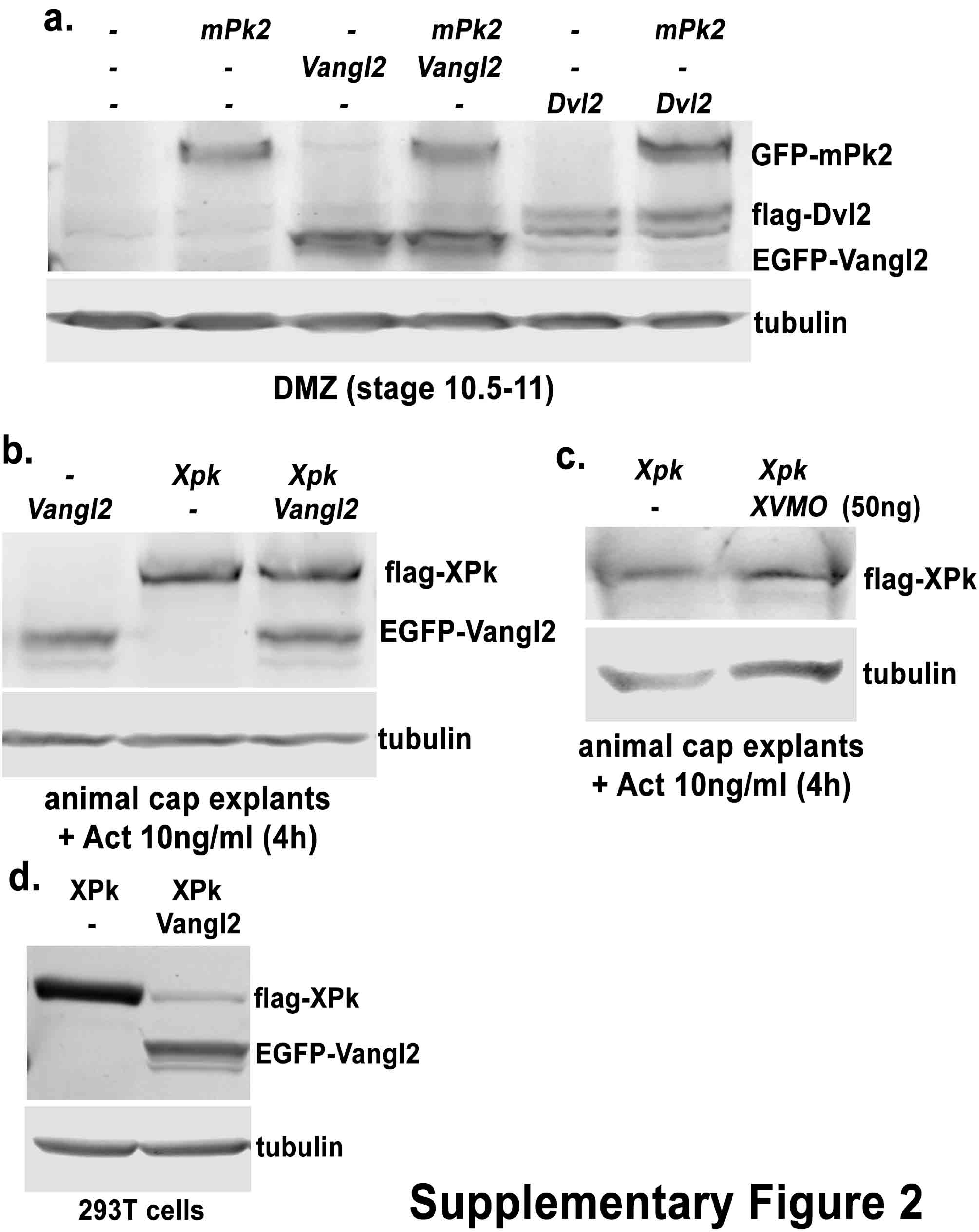
a.
-
mPk2
-
mPk2
-
mPk2
-
-
Vangl2
Vangl2
-
-
-
-
-
-
Dvl2
Dvl2
GFP-mPk2
flag-Dvl2
EGFP-Vangl2
tubulin
DMZ (stage 10.5-11)
b.
-
Xpk
Xpk
Vangl2
-
Vangl2
flag-XPk
EGFP-Vangl2
tubulin
animal cap explants
+ Act 10ng/ml (4h)
c.
Xpk
Xpk
-
XVMO (50ng)
flag-XPk
tubulin
animal cap explants
+ Act 10ng/ml (4h)
d.
XPk
XPk
-
Vangl2
flag-XPk
EGFP-Vangl2
tubulin
293T cells

Supplementary Figure 2

a. GFPmPk2
b. GFPmPk2+mVangl2
c. GFPmPk2
d. GFPmPk2+XVMO (30ng)
e. GFPmPk2+XVMO (30ng)
+mVangl2 (50pg)

Supplementary Figure 3

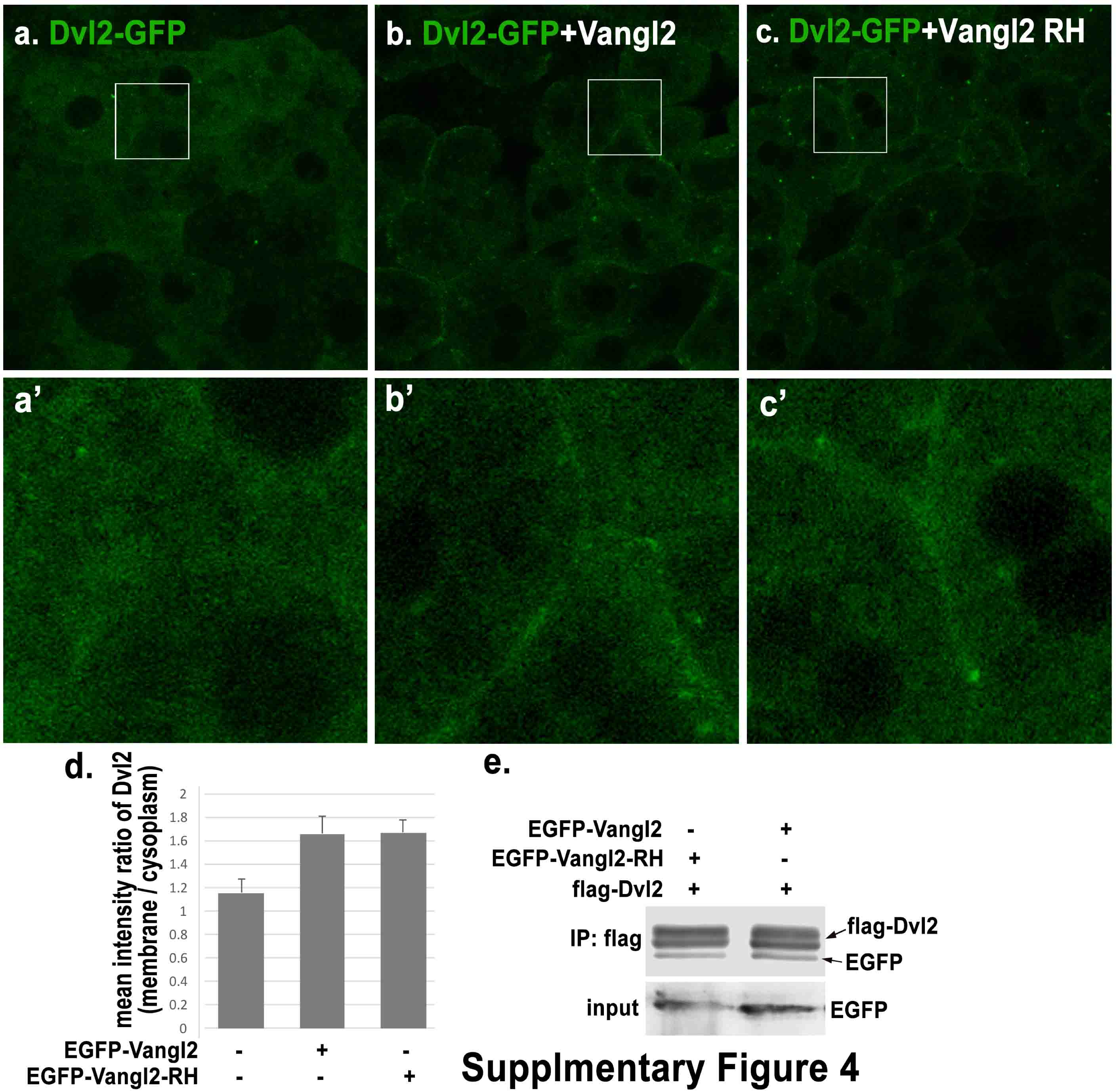
a. Dvl2-GFP
b. Dvl2-GFP+Vangl2
c. Dvl2-GFP+Vangl2 RH
a’
b’
c’
d.
mean intensity ratio of Dvl2
(membrane / cysoplasm)
2
1.8
1.6
1.4
1.2
1
0.8
0.6
0.4
0.2
0
EGFP-Vangl2 - + -
EGFP-Vangl2-RH - - +
e.
EGFP-Vangl2 - +
EGFP-Vangl2-RH + -
flag-Dvl2 + +
IP: flag
flag-Dvl2
EGFP
input
EGFP

Supplmentary Figure 4

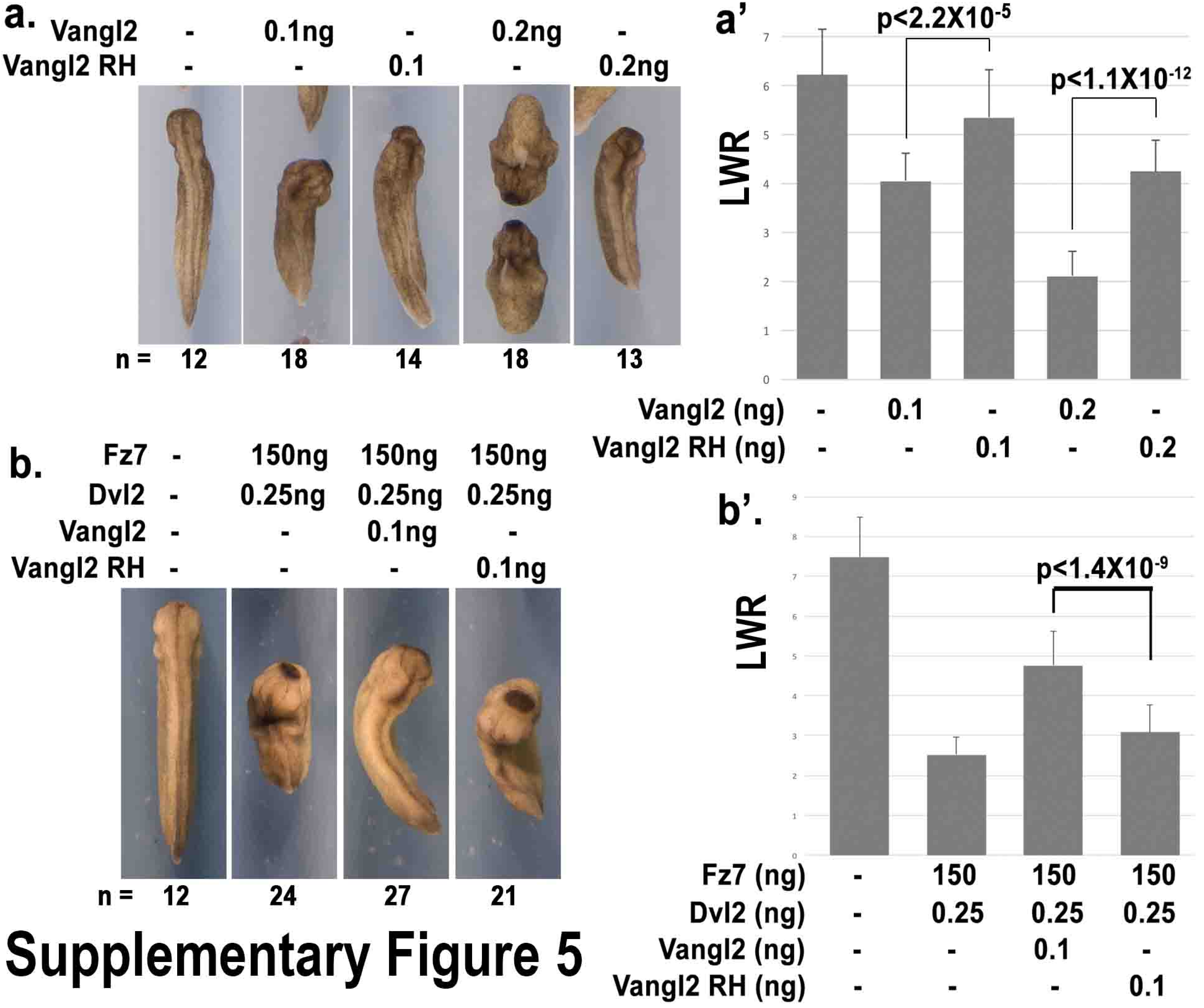

Supplementary Figure 5

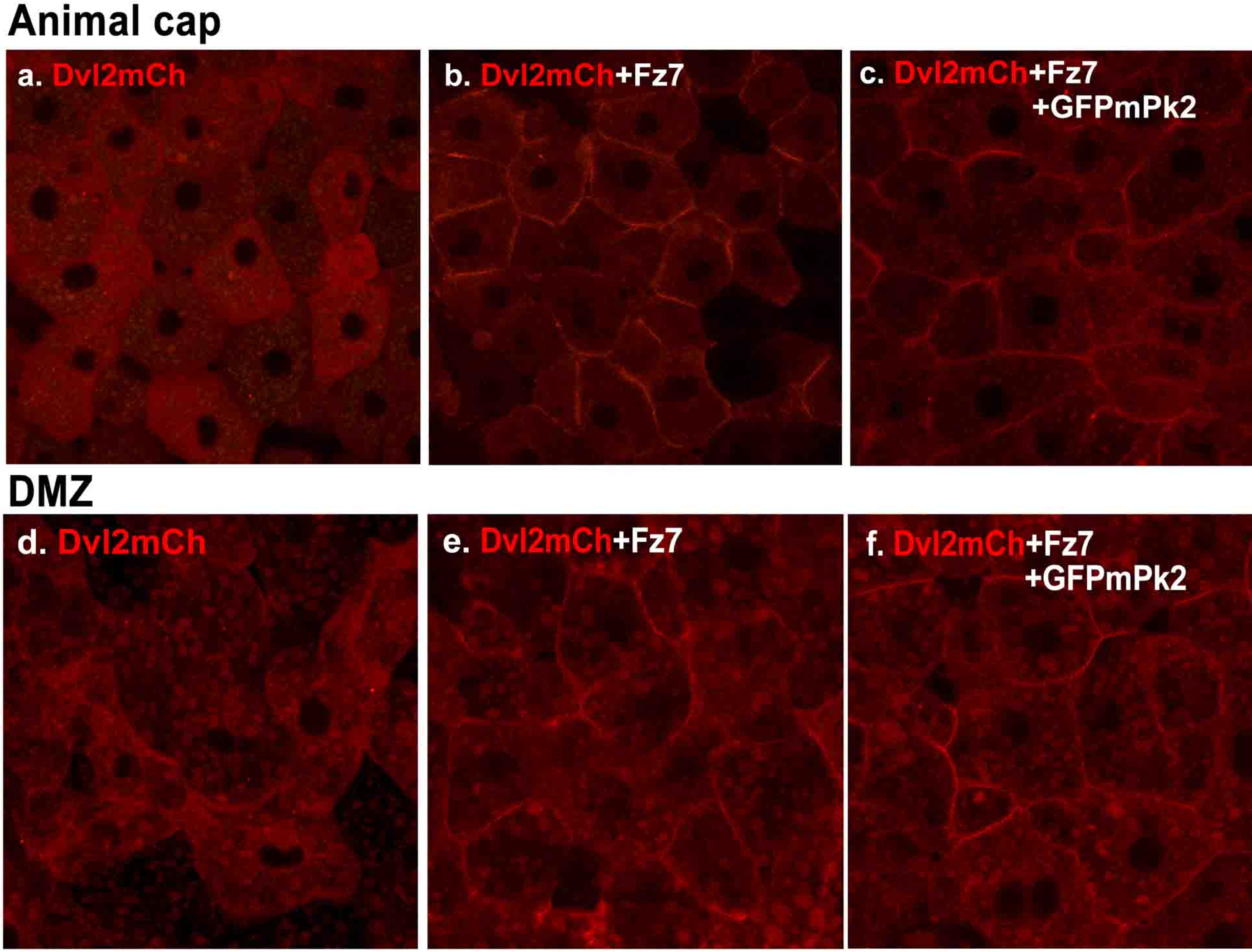
Animal cap
a. Dvl2mCh
b. Dvl2mCh+Fz7
c. Dvl2mCh+Fz7
+GFPmPk2
DMZ
d. Dvl2mCh
e. Dvl2mCh+Fz7
f. Dvl2mCh+Fz7
+GFPmPk2

Supplementary Figure 6

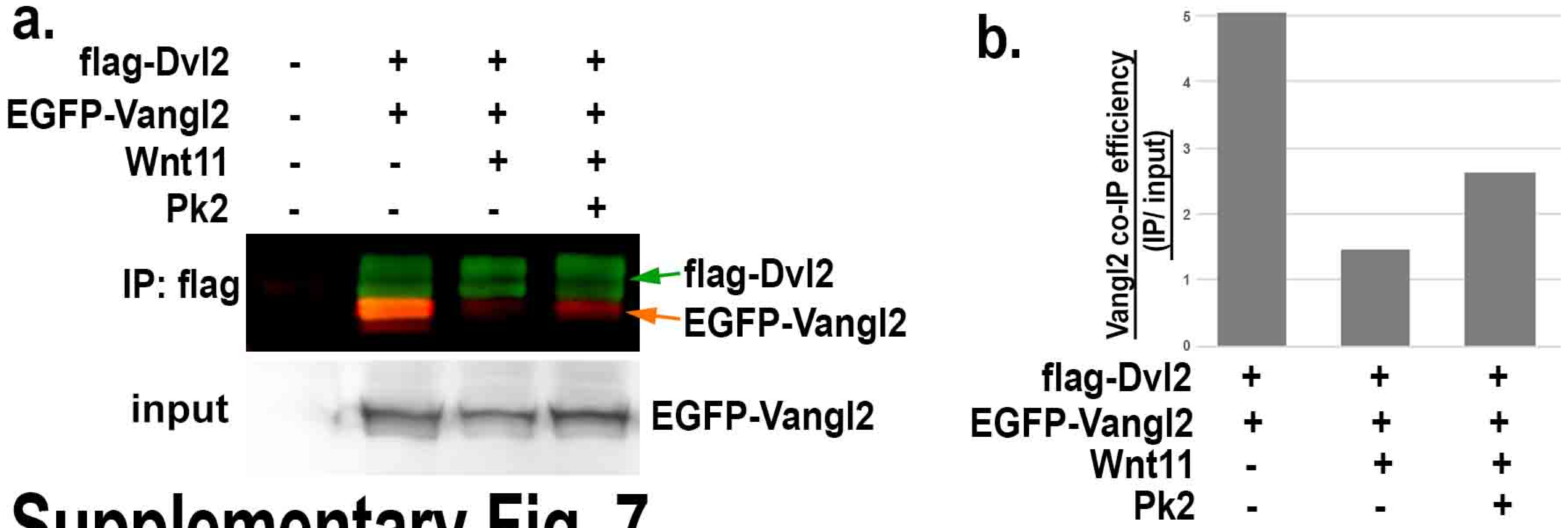

Supplementary Fig. 7

a. EGFP-Vangl2 (0.1ng)
Wnt11
Dvl2mCh
b. EGFP-Vangl2 (0.1ng)
Wnt11
Dvl2mCh
c. EGFP-Vangl2 (0.1ng)
Wnt11
Dvl2mCh
a'. EGFP-Vangl2 (0.1ng)
Wnt11
Dvl2mCh
b'. EGFP-Vangl2 (0.1ng)
Wnt11
Dvl2mCh
c'. EGFP-Vangl2 (0.1ng)
Wnt11
Dvl2mCh

Supplmentary Figure 8

a. Fz7-GFP+FM4-64FX
b. Fz7-GFP+FM4-64FX
c. Fz7-GFP+FM4-64FX
a’
b’
c’
d. Fz7-GFP+FM4-64FX
+HA-Vang2/Pk
e. Fz7-GFP+FM4-64FX
+HA-Vangl2/Pk
f. Fz7-GFP+FM4-64FX
+HA-Vangl2/Pk
d’
e’
f’

Supplementary Figure 9

a. Fz7-GFP+Wnt11
b. Fz7-GFP+Wnt11+DshMA

Supplementary Figure 10

a
Vangl2 - 0.2ng 0.2ng 0.2ng -
Ror2 - - 0.05ng 0.1ng 0.1ng
n = 16 13 16 19 15
b
LWR
9
8
7
6
5
4
3
2
1
0
P=0.00002
P=0.07
Vangl2 (ng) - 0.2 0.2 0.2 -
Ror2 (ng) - - 0.05 0.1 0.1

Supplementary Figure 11. Ror2 antagonizes Vangl2 during CE

Supplementary Fig. 12